

## Article

# Consecutive Multicomponent Coupling-Addition Synthesis and Chromophore Characteristics of Cyclohexene-Embedded Merocyanines and Cyanines

Julian Papadopoulos <sup>1</sup>, Tabea Gerlach <sup>1</sup>, Guido J. Reiss <sup>2</sup> , Bernhard Mayer <sup>1</sup> and Thomas J. J. Müller <sup>1,\*</sup> 

<sup>1</sup> Institut für Organische Chemie und Makromolekulare Chemie, Heinrich-Heine-Universität Düsseldorf, Universitätsstraße 1, D-40225 Düsseldorf, Germany

<sup>2</sup> Institut für Anorganische Chemie und Strukturchemie, Heinrich-Heine-Universität Düsseldorf, Universitätsstraße 1, D-40225 Düsseldorf, Germany

\* Correspondence: ThomasJJ.Mueller@hhu.de

**Abstract:** Merocyanines with embedded butadiene structure in a cyclohexane scaffold are readily obtained by consecutive three-component alkynylation-addition sequences in moderate to excellent yield. Moreover, employing pyrrolidine as an amine provides a pseudo four-component synthesis of related cyanines by carbonyl condensation of the heterocyclic amine in excellent yield. While the merocyanines are essentially nonluminescent, pentamethine cyanines show luminescence with low quantum yield. TDDFT calculations using various exchange correlation hybrid functionals in the gas phase and explicit continuum of dichloromethane underline that the lowest energy absorption bands are highly solvent dependent for a merocyanine and cyanine model. The blue-shifted deviation from the experimental spectra agrees with related merocyanine and cyanine systems. The lowest energy absorption band of merocyanines contains  $n\text{-}\pi^*$  character, which rationalizes the absence of luminescence.

**Keywords:** cross-coupling; cyanines; DFT calculations; merocyanines; multicomponent reactions



**Citation:** Papadopoulos, J.; Gerlach, T.; Reiss, G.J.; Mayer, B.; Müller, T.J.J. Consecutive Multicomponent Coupling-Addition Synthesis and Chromophore Characteristics of Cyclohexene-Embedded Merocyanines and Cyanines. *Photochem* **2022**, *2*, 672–693. <https://doi.org/10.3390/photochem2030044>

Academic Editor: Rui Fausto

Received: 14 July 2022

Accepted: 16 August 2022

Published: 19 August 2022

**Publisher's Note:** MDPI stays neutral with regard to jurisdictional claims in published maps and institutional affiliations.



**Copyright:** © 2022 by the authors. Licensee MDPI, Basel, Switzerland. This article is an open access article distributed under the terms and conditions of the Creative Commons Attribution (CC BY) license (<https://creativecommons.org/licenses/by/4.0/>).

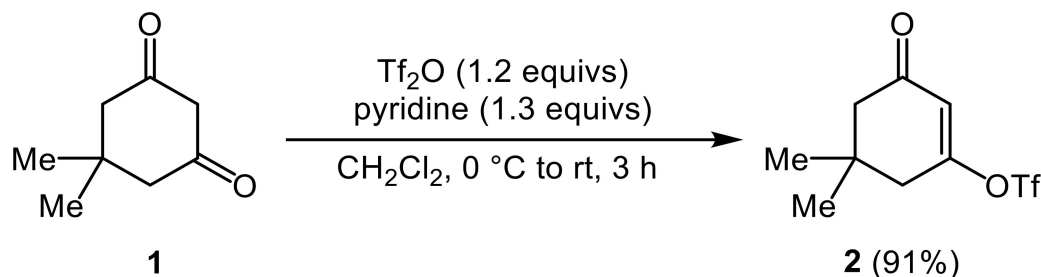
## 1. Introduction

Merocyanines [1–6] are structurally characterized as neutral polymethines possessing high extinction coefficients and as highly polarizable  $\pi$ -electron systems. This sets the stage for applications in optoelectronics [7–10], organic semiconductors [11], and photovoltaics [12]. Due to their polar nature and polarizability, their self-assembly in solution enables access to nanoscale objects and supramolecular materials [13,14]. Classical synthetic approaches to merocyanines and many polymethine dyes are conventional aldol or Knoevenagel condensations [1,15–17]. More modern concepts for the synthesis of functional chromophores, such as fluorophores and electrophores [18–20] with heterocyclic scaffolds rely on multicomponent reactions (MCR) [21–24] and domino processes [25,26]. In particular, generating alkynoyl intermediates as part of the catalytic entry to MCR [27] paved the way to several fluorophores in a modular one-pot fashion [28]. In recent years, we have reported concise consecutive three-component syntheses of luminescent merocyanine luminophores based upon an alkynylation-addition sequence [29,30]. Upon derivatization, the merocyanines could also be embedded as covalently bound constituents in highly fluorescent PMMA copolymers [31]. Encouraged by the three-component synthesis of coumarin based luminophores and the tunability of their electronic properties already at the stage of the alkynyl coumarin intermediates [32], we reasoned that the interesting electronic properties of cyclohexanone-based merocyanines as previously shown by Laschat's group [33] could be valuable targets for an MCR approach based upon our alkynylation-addition strategy. Here, we report the concise consecutive three-component synthesis of cyclohexanone-based merocyanines and the pseudo four-component synthesis of selected cyanines and the investigation of their UV/Vis absorption properties.

## 2. Results and Discussion

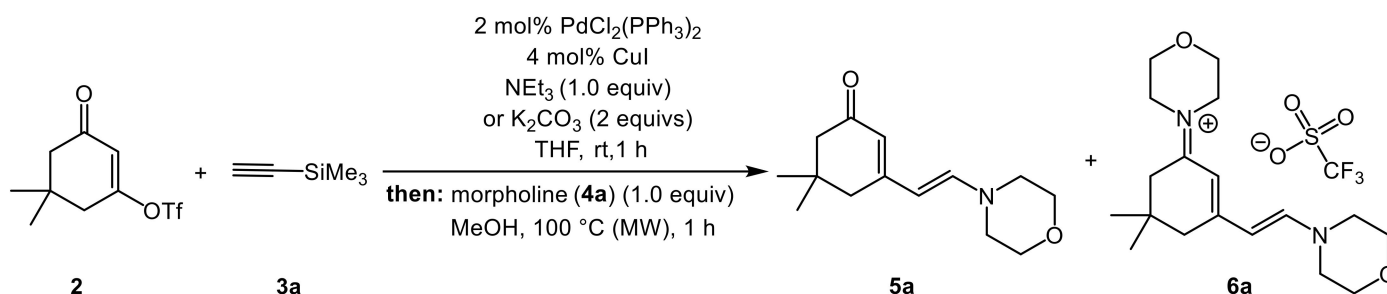
### 2.1. Synthesis and Structure

Starting from dimedone (**1**), i.e., 5,5-dimethylcyclohexane-1,3-dione, a suitable (pseudo) halide is generated by reaction with triflic anhydride to give the corresponding triflate **2** in excellent yield according to the literature (Scheme 1) [34,35].



**Scheme 1.** Synthesis of triflate **2**.

Based upon our experience with alkynylation of coumarin triflates [32] and their use in consecutive three-component alkynylation-addition sequences [30], we first set out to probe the same reaction conditions in a model reaction of triflate **2**, (trimethylsilyl)acetylene (**3a**), and morpholine (**4a**). To our surprise a mixture of the merocyanine **5a** and the cyanine **6a** is formed upon heating to 100 °C in the microwave cavity for 1 h, if triethylamine is employed as a base (Scheme 2, Table 1). While merocyanine **5a** can be isolated upon flash chromatography, cyanine **6a** is only identified in an inseparable fraction by the mass peaks of the cation and the triflate in the HRMS (Table 1, entries 1–3). However, no product is obtained upon altering the base of the alkynylation step to Hünig's base (DIPEA) (Table 1, entry 4), while employing potassium carbonate (Table 1, entries 5 and 6) exclusively produces the merocyanine **5a**.



**Scheme 2.** Multi-component formation of merocyanine **5a** and cyanine **6a**.

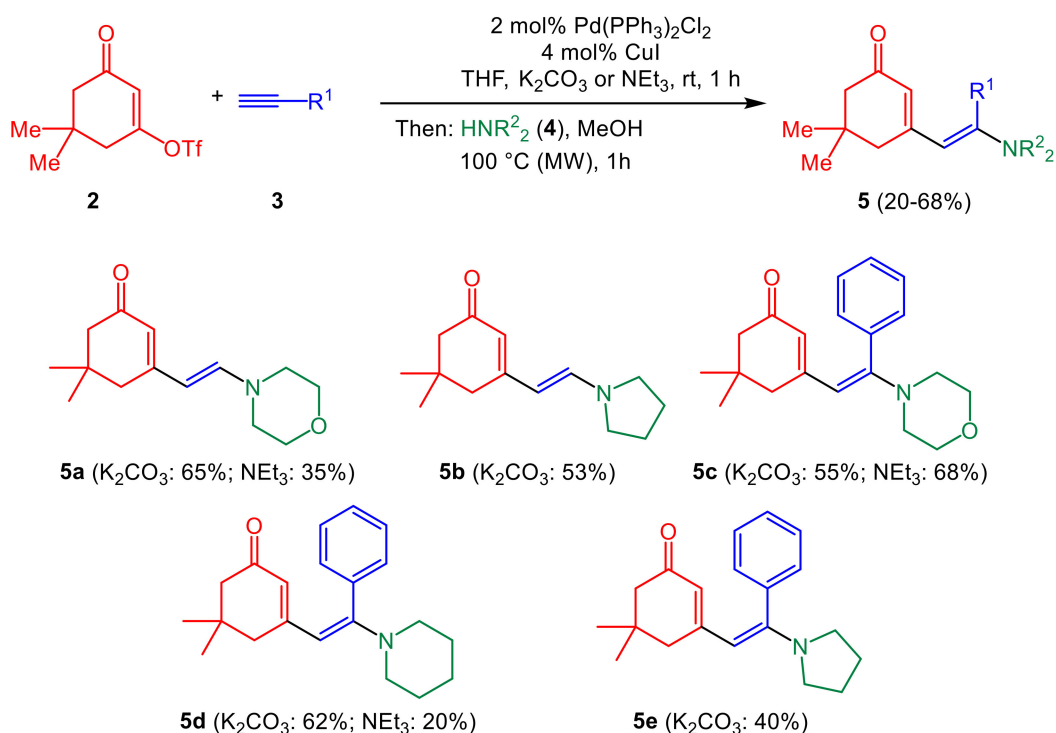
**Table 1.** Effect of the base on the multi-component formation of merocyanine **5a** and cyanine **6a**.

Entry	Base	Morpholine (4a) [Equivs]	Temperature [°C]	Reaction Time [h]	Merocyanine 5a <sup>a</sup>	Cyanine 6a <sup>b</sup>
1	NEt <sub>3</sub>	1	100 (MW)	1	35%	+
2	NEt <sub>3</sub>	2	100 (MW)	1	21%	+
3	NEt <sub>3</sub>	1	rt	18	n.d.	+
4	DIPEA	1	100 (MW)	1	n.d.	n.d.
5	K <sub>2</sub> CO <sub>3</sub> <sup>c</sup>	1	100 (MW)	1	65%	n.d.
6	K <sub>2</sub> CO <sub>3</sub> <sup>c</sup>	1	RT	21	67%	n.d.

<sup>a</sup> Yield after chromatography on silica gel, n.d.: not detected on TLC. <sup>b</sup> The product is impure after chromatography on silica gel, but identified by HRMS in the fraction, n.d.: not detected on TLC. <sup>c</sup> K<sub>2</sub>CO<sub>3</sub> (2 equivs) is employed as a base and the reaction time of the alkynylation step is 2 h.

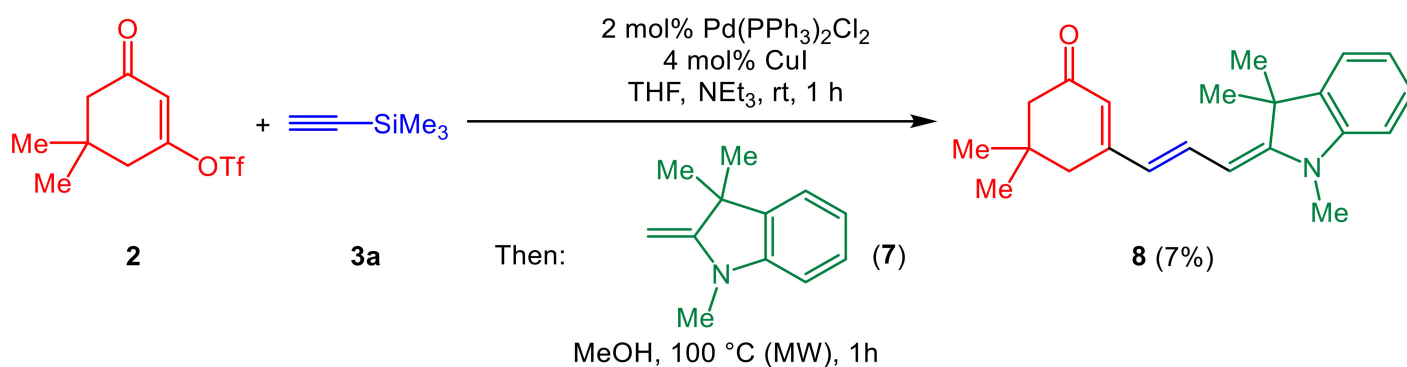
Starting from triflate **2**, alkyne **3**, and heterocyclic secondary amine **4**, potassium carbonate and triethylamine can both be successfully employed in the alkynylation step of

the three-component syntheses of merocyanines **5**; however, in most cases the former base gives higher yields after isolation by flash chromatography (Scheme 3).



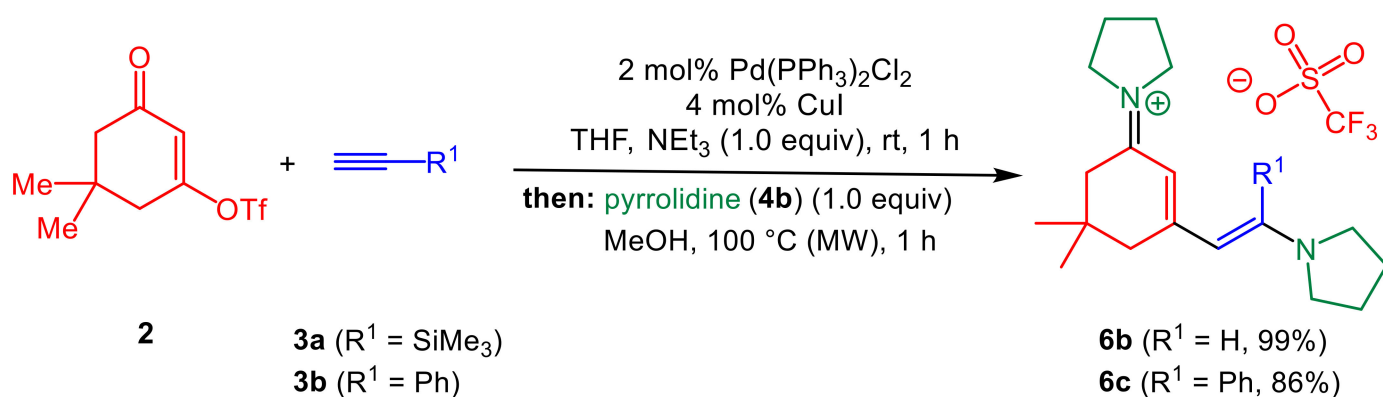
**Scheme 3.** Three-component synthesis of merocyanines **5** employing potassium carbonate or triethylamine as a base in the alkynylation step.

Moreover, Fischer's base (**7**) can be employed in the addition step of the consecutive merocyanine synthesis using triethylamine as the base in the alkynylation step, albeit, with only a poor overall yield of merocyanine **8** (Scheme 4).



**Scheme 4.** Three-component synthesis of merocyanine **8**.

Intrigued by the formation of cyanine **6a** as a byproduct and employing pyrrolidine (**4b**) as a stronger nucleophile, we set out to probe the selective formation of cyanines **6** in a pseudo four-component fashion. Indeed, upon reaction of triflate **2**, alkynes **3** ( $\text{R}^1 = \text{SiMe}_3$  or Ph), and pyrrolidine (**4b**) in the presence of triethylamine as a base in the alkynylation step, cyanines **6** is obtained analytically pure and in excellent yield as triflate salts after chromatography on silica gel (Scheme 5). It is noteworthy to mention that piperidine (**4c**) is obviously not nucleophilic enough to give complete conversion to the corresponding cyanine, which is only identified in the inseparable fraction after flash chromatography.



**Scheme 5.** Pseudo four-component synthesis of cyanines **6**.

The structures of the merocyanines **5** and **8** and the cyanines **6** were unambiguously assigned by NMR spectroscopy and mass spectrometry. The representative discussion of extensive NMR spectroscopy of compound **5e** underlines some features of the merocyanines. The geminal methyl groups on the cyclohexenone moiety appear as a singlet at  $\delta$  0.79, indicating the overall planar structure of the merocyanine chromophore in solution (Figure 1). The methylene protons in  $\alpha$ - and  $\gamma$ -position to the carbonyl group appear as singlets at  $\delta$  2.01 and 1.65. Methine signals for the  $\alpha$ - and the  $\gamma$ -positions of the Michael system are expectedly found a higher field and appear as singlets at  $\delta$  5.05 and 5.41. The methylene protons of the pyrrolidinyl moiety are not well resolved and are found at  $\delta$  1.89 and 3.15.

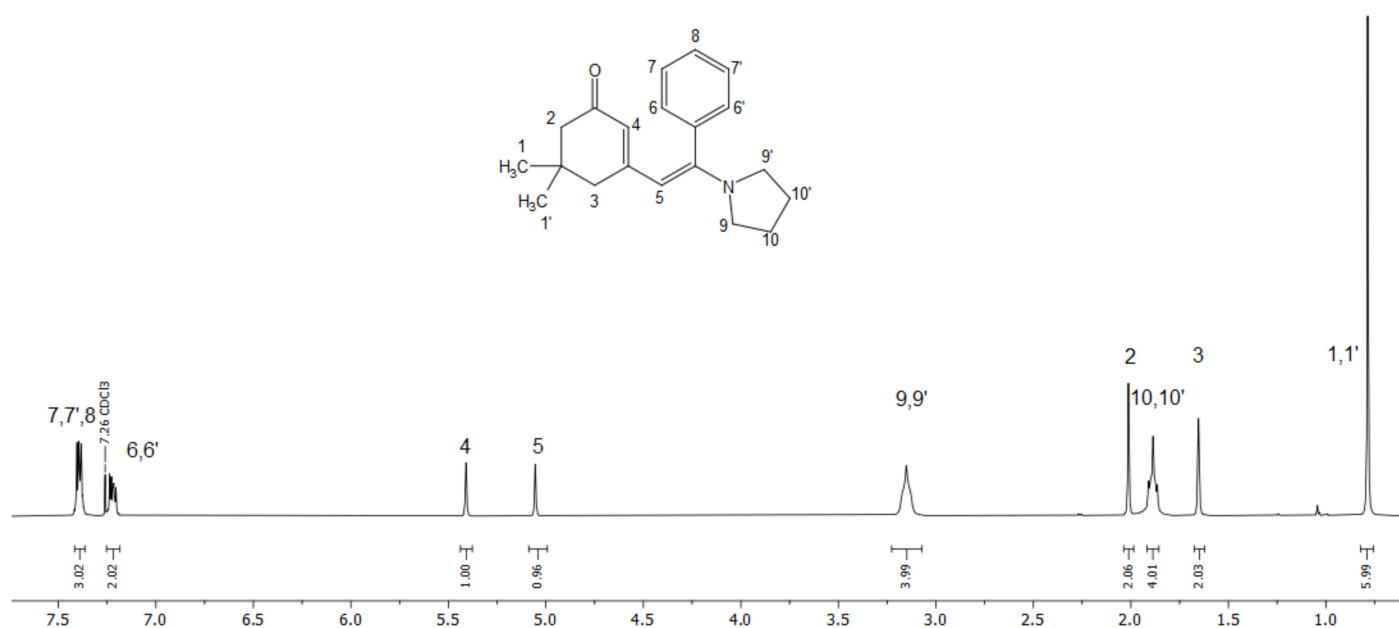


**Figure 1.**  $^1\text{H}$  NMR spectrum of compound **5e** ( $\text{CDCl}_3$ , 300 MHz, 298 K).

The *E*-configuration of the pyrrolidinyl vinyl substituent can be assigned by the NOESY spectrum, where the pyrrolidinyl  $\alpha$ -protons at  $\delta$  3.15 and the cyclohexenyl methylene protons at  $\delta$  1.65 give cross-peaks to the merocyanine methine proton at  $\delta$  5.05 (Figure 2).

In addition, the structure of cyanine **6b** was corroborated by an X-ray structure analysis (Figure 3) [36], which clearly shows that an *E*-configured isomer was formed in the synthesis. Furthermore, the inspection of the bond lengths of the fully planarized pentamethine part of the chromophore supports the highly delocalized cyanine structure with a small bond length alternation [37] of 0.027 Å for the bonds C1-C6, C6-C5, C5-C7, and C7-C8 (Table 2,



entries 2–5), which is typical for nearly symmetrical electron density distribution in cationic cyanine dyes [38].

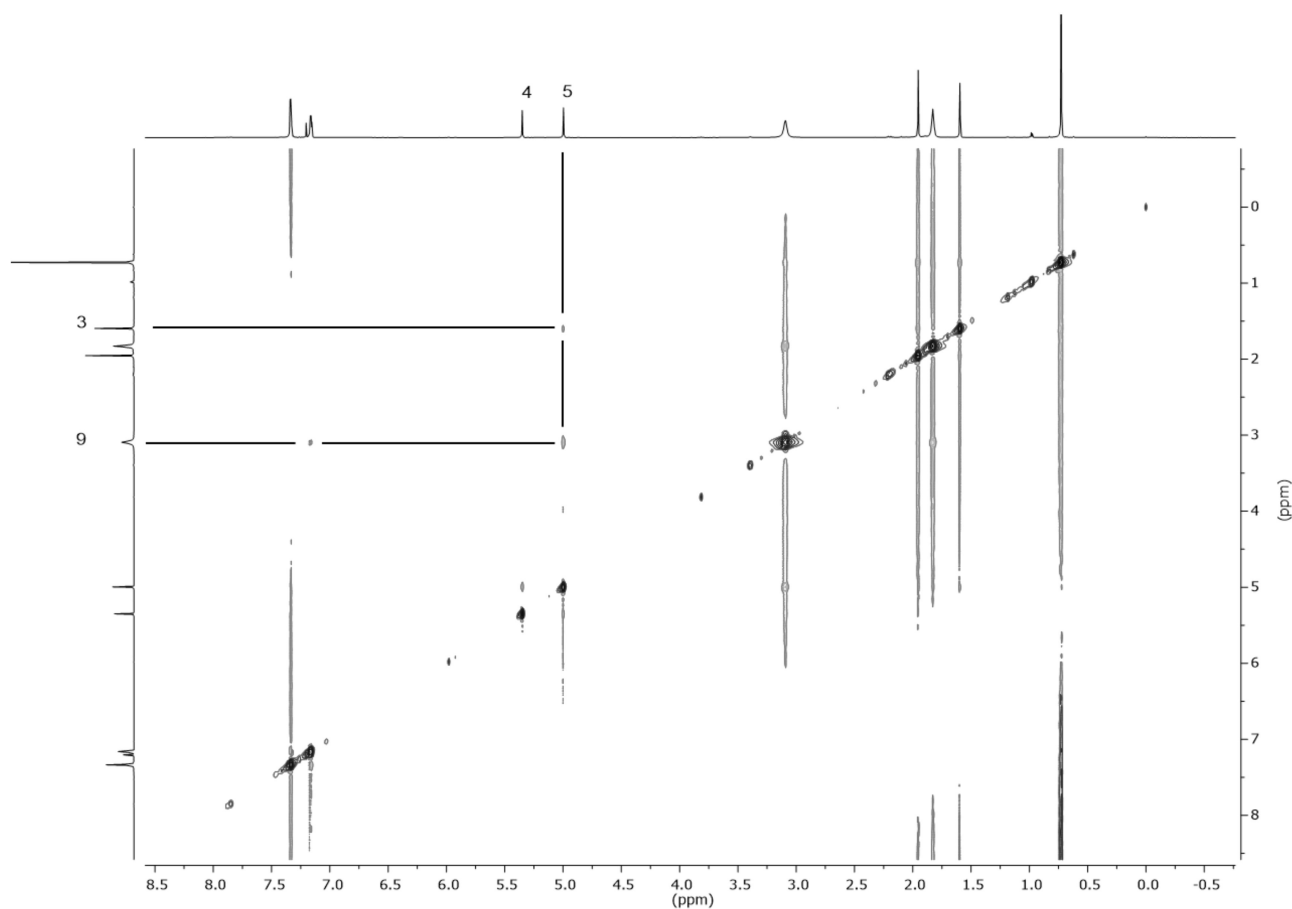


**Figure 2.** NOESY spectrum of compound **5e** (CDCl<sub>3</sub>, 600 MHz, 298 K).

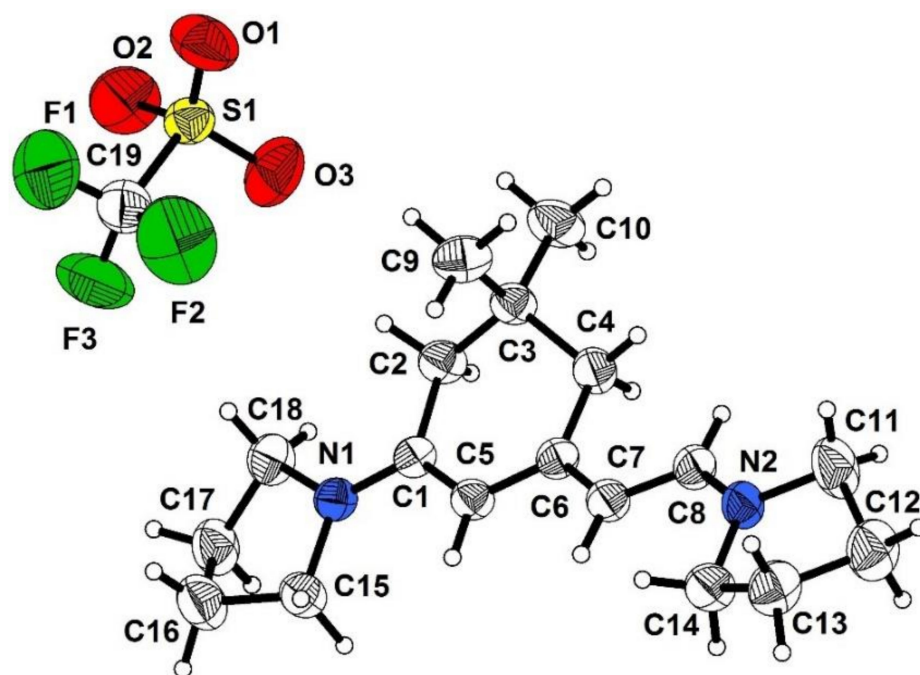


**Figure 3.** Molecular structure of **6b**. Displacement ellipsoids are drawn at the 50% probability level; H atoms are drawn with an arbitrary radius.

**Table 2.** Selected bond lengths of structure **6b**.

Entry	Bond	Bond Length [Å]
1	N1-C1	1.316
2	C1-C6	1.399
3	C6-C5	1.380
4	C5-C7	1.404
5	C7-C8	1.369
6	C8-N6	1.320

## 2.2. Absorption and Emission Characteristics

Merocyanines **5** and **8** and cyanines **6** that are obtained as yellow to orange solids were investigated by UV/Vis and emission spectroscopy in dichloromethane solution (Table 3). The merocyanines **5** give typically broad, unstructured longest wavelength absorption bands between 365 and 388 nm (Figure 4, Table 3, entries 1–5), also revealing that the maxima redshift with increasing electron donicity of the secondary amine from morpholine over piperidine to pyrrolidine. Extension of the  $\pi$ -system as for merocyanine **8** expectedly causes a redshift of the absorption band to 442 nm (Table 3, entry 6). The absorption solvatochromicity in qualitative UV/Vis measurements is small, similarly as reported for more rigidified merocyanines [33] accounting for a more polyene-like ground state structure of merocyanines **5** and **8**. None of the merocyanines, neither **5** nor **8**, display any emission upon detection with the naked eye and attempted emission spectroscopy also remains unsuccessful. The cyanines **6b** and **6c** possess cyanine typical narrow absorption bands at 443 and 459 nm with absorption coefficients exceeding  $10^5 \text{ M}^{-1}\text{cm}^{-1}$  (Figure 5, Table 3, entries 7 and 8). Both cyanines are weakly emissive with a sharp emission maximum at 453 nm for cyanine **6b**, indicating minimal structural changes in the vibrationally relaxed  $S_1$  after photonic excitation, and a broad emission maximum at 513 nm for cyanine **6c**. The latter large Stokes shift of  $2300 \text{ cm}^{-1}$  accounts for more pronounced structural changes upon electronic excitation from the electronic ground state  $S_0$  to the vibrationally relaxed  $S_1$ .

**Table 3.** Absorption and emission characteristics of selected merocyanines **5** and **8** and cyanines **6** (recorded in  $\text{CH}_2\text{Cl}_2$  at  $T = 293 \text{ K}$ ).

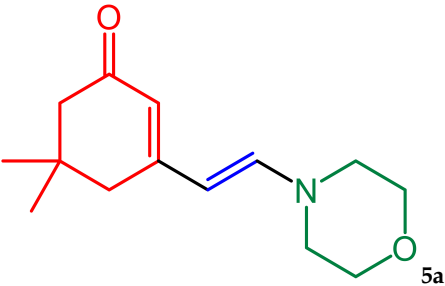
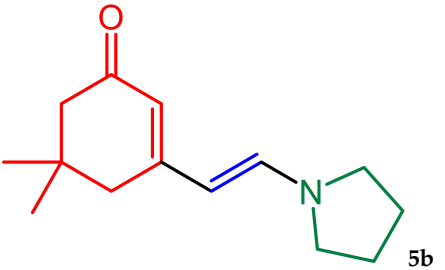
Entry	Compound	$\lambda_{\text{max,abs}} [\text{nm}]^a (\epsilon [\text{M}^{-1}\text{cm}^{-1}])$	$\lambda_{\text{max,em}} [\text{nm}]^b$	Stokes Shift $\Delta\tilde{\nu} [\text{cm}^{-1}]^c$
1	 5a	373 (71,000)	n.d. <sup>d</sup>	
2	 5b	373 (71,000)	n.d. <sup>d</sup>	

Table 3. Cont.

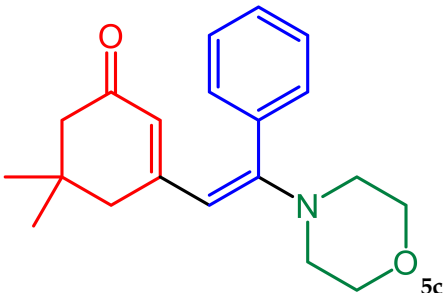
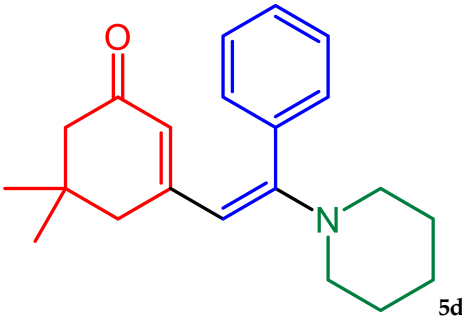
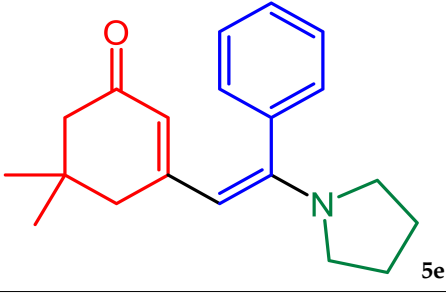
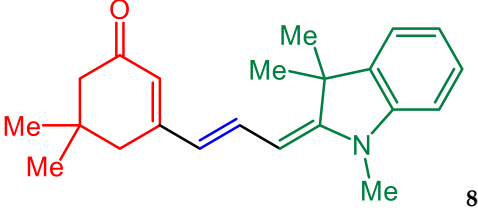
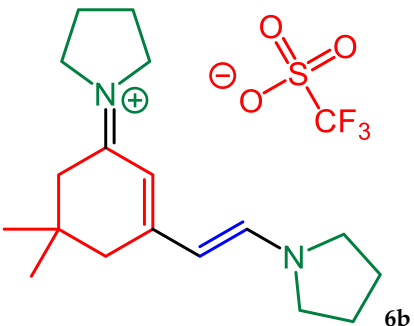
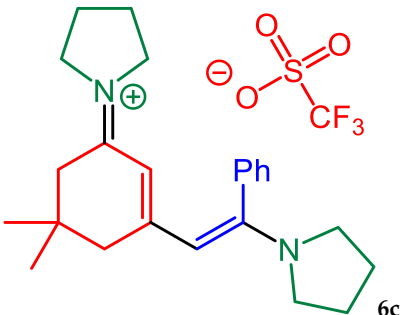
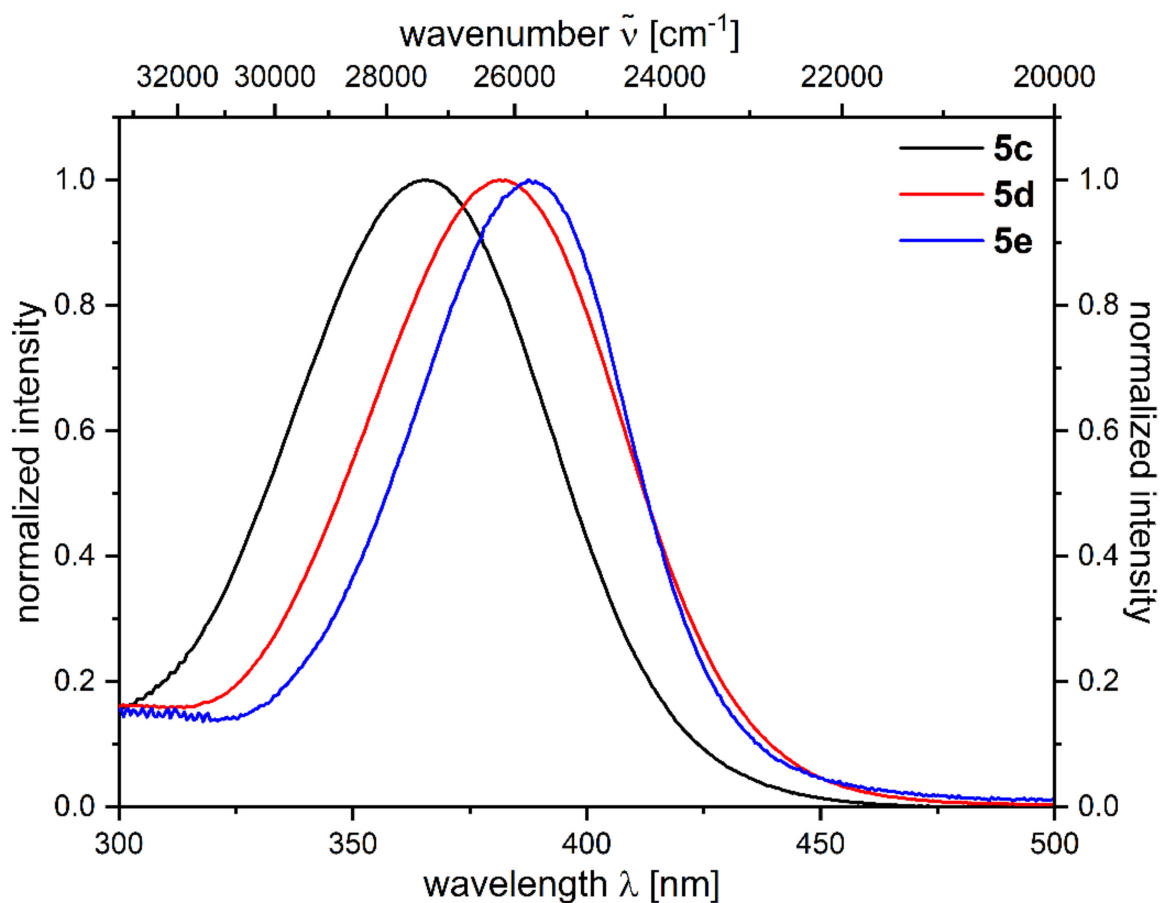
Entry	Compound	$\lambda_{\text{max,abs}}$ [nm] <sup>a</sup> ( $\epsilon$ [M <sup>-1</sup> cm <sup>-1</sup> ])	$\lambda_{\text{max,em}}$ [nm] <sup>b</sup>	Stokes Shift $\Delta\tilde{\nu}$ [cm <sup>-1</sup> ] <sup>c</sup>
3	 5c	365 (19,000)	n.d. <sup>d</sup>	
4	 5d	383 (22,000)	n.d. <sup>d</sup>	
5	 5e	388 (43,000)	n.d. <sup>d</sup>	
6	 8	442 (27,000)	n.d. <sup>d</sup>	
7	 6b	443 (114,000)	459	800

Table 3. Cont.

Entry	Compound	$\lambda_{\max, \text{abs}}$ [nm] <sup>a</sup> ( $\epsilon$ [M <sup>-1</sup> cm <sup>-1</sup> ])	$\lambda_{\max, \text{em}}$ [nm] <sup>b</sup>	Stokes Shift $\Delta\tilde{\nu}$ [cm <sup>-1</sup> ] <sup>c</sup>
8	 6c	459 (130,000)	513	2300

<sup>a</sup> Longest wavelength absorption maximum. <sup>b</sup> Emission maximum. <sup>c</sup>  $\Delta\tilde{\nu} = 1/\lambda_{\max, \text{abs}} - 1/\lambda_{\max, \text{em}}$  [cm<sup>-1</sup>].  
<sup>d</sup> Not detected.



**Figure 4.** Normalized absorption spectra of merocyanines 5c–e (recorded in dichloromethane,  $c(5) = 10^{-5}$  M,  $T = 298$  K).

### 2.3. Calculated Electronic Structure

For assigning the photophysical characteristics of merocyanines 5 and cyanines 6, calculations of the UV/Vis transitions of geometry optimized structures of merocyanine 5b and cyanine 6b were performed on the DFT and TDDFT level of theory using various exchange correlation hybrid functionals (B3LYP [39], PBEh1PBE [40], and CAM-B3LYP [41]) and the 6-311++G\*\* basis set [42], which was chosen to most precisely describe polarization as well as long-range interactions. Besides gas phase calculations, the polarizable contin-

uum model (PCM) for the dichloromethane as a dielectric continuum is employed [43] as implemented in the program package Gaussian 16 [44]. The comparative calculations of the first excited states  $S_1$  to  $S_6$  are summarized in Table 4 (merocyanine **5b**) and Table 5 (cyanine **6b**). The longest wavelength absorption bands possess high extinction coefficients in the experimental spectra and this aspect is mirrored by high oscillatory strengths in the calculated spectra (see Supplementary Materials).

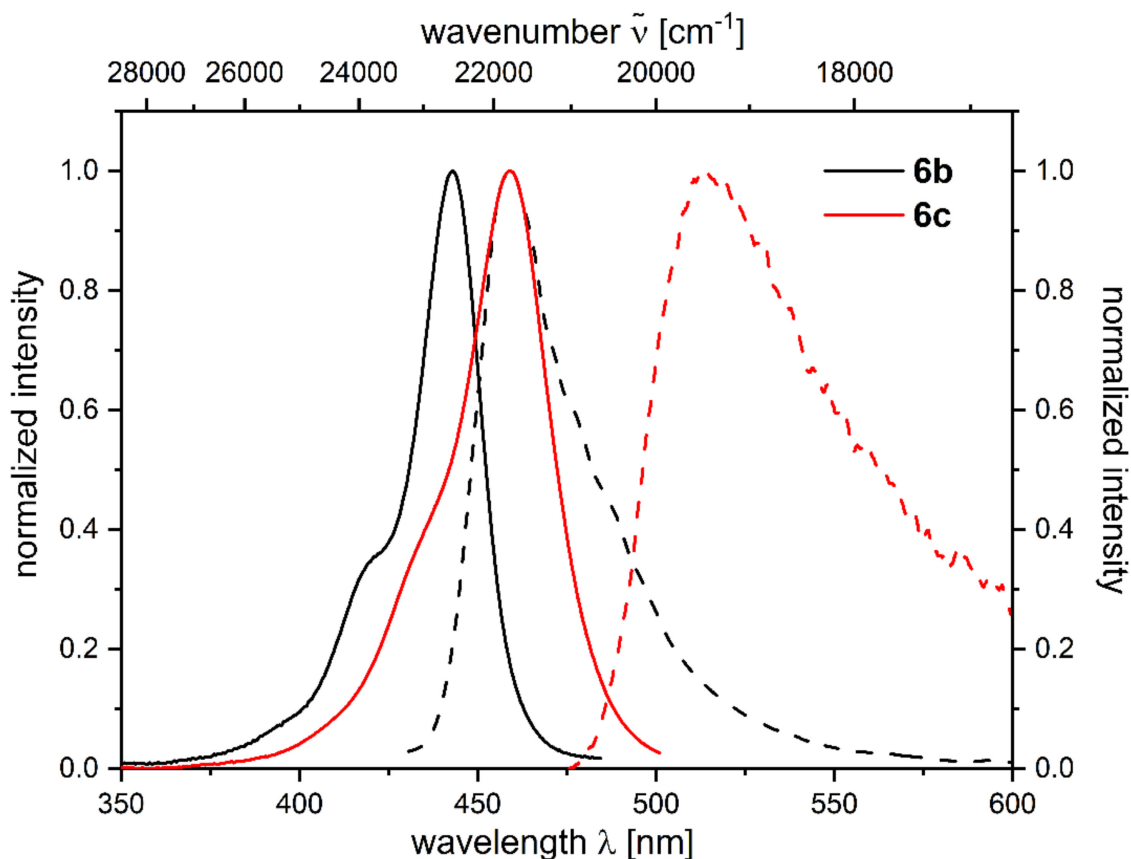


**Figure 5.** Normalized absorption and emission spectra of cyanines **6b** and **6c** (recorded in dichloromethane,  $c(6) = 10^{-5}$  M,  $T = 298$  K).

**Table 4.** Experimentally determined longest wavelength absorption band (recorded in dichloromethane at  $T = 298$  K) and TDDFT calculated absorption spectra of merocyanine **5b** using various functionals and 6-311++G\*\* as a basis set.

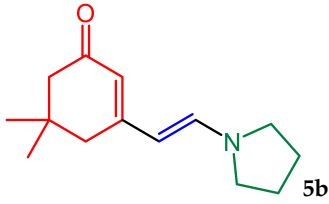
		$\lambda_{\max, \text{abs exp}} 373 \text{ nm}/3.327 \text{ eV} (71,000 \text{ M}^{-1} \text{cm}^{-1})$				
Functional	State	$\lambda_{\max, \text{abs calcd}}$ [nm]	[eV]	Oscillatory Strength $f$	Most Dominant Contribution (%)	$\Delta E_{\text{calcd-exp}}$ [eV]
B3LYP <sup>a</sup>	$S_1$	361.0	3.426	0.0077	HOMO-1 $\rightarrow$ LUMO (92%) HOMO $\rightarrow$ LUMO (2%)	0.400
	$S_2$	331.8	3.727	0.6853	HOMO $\rightarrow$ LUMO (97%) HOMO-1 $\rightarrow$ LUMO (2%)	
	$S_3$	302.6	4.087	0.0137	HOMO $\rightarrow$ LUMO+1 (97%)	

Table 4. Cont.

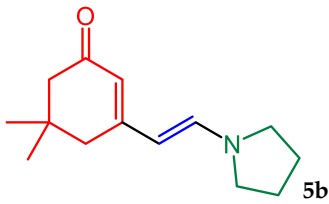
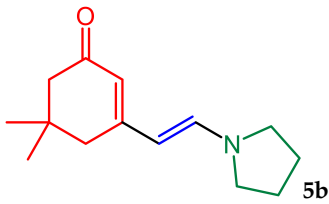
		$\lambda_{\text{max,abs exp}} 373 \text{ nm}/3.327 \text{ eV} (71,000 \text{ M}^{-1}\text{cm}^{-1})$				
Functional	State	$\lambda_{\text{max,abs calcd}}$		Oscillatory	Most Dominant	$\Delta E_{\text{calcd-exp}}$
		[nm]	[eV]	Strength $f$	Contribution (%)	[eV]
B3LYP (CH <sub>2</sub> Cl <sub>2</sub> ) <sup>b</sup>	S <sub>4</sub>	272.3	4.542	0.002	HOMO→LUMO+2 (91%)	0.127
	S <sub>5</sub>	264.5	4.676	0.004	HOMO→LUMO+3 (5%)	
	S <sub>6</sub>	257.9	4.796	0.0157	HOMO→LUMO+3 (83%)	
					HOMO→LUMO+2 (5%)	
					HOMO→LUMO+4 (93%)	
					HOMO→LUMO+3 (4%)	
	S <sub>1</sub>	358.1	3.454	0.8517	HOMO→LUMO (99%)	0.127
	S <sub>2</sub>	336.1	3.680	0.0094	HOMO-1→LUMO (95%)	
	S <sub>3</sub>	280.8	4.405	0.0128	HOMO→LUMO+1 (96%)	
					HOMO→LUMO+5 (3%)	
	S <sub>4</sub>	261.2	4.736	0.0059	HOMO→LUMO+2 (97%)	
	S <sub>5</sub>	253.2	4.884	0.0033	HOMO→LUMO+3 (67%)	
	S <sub>6</sub>	247.1	5.006	0.0366	HOMO→LUMO+4 (28%)	0.276
					HOMO→LUMO+4 (64%)	
B3LYP (CH <sub>2</sub> Cl <sub>2</sub> ) <sup>c</sup>	S <sub>1</sub>	345.0	3.603	0.7163	HOMO→LUMO (94%)	0.276
					HOMO-1→LUMO (5%)	
					HOMO-1→LUMO (90%)	
	S <sub>2</sub>	334.8	3.694	0.0522	HOMO→LUMO (6%)	0.596
					HOMO→LUMO+1 (96%)	
	S <sub>3</sub>	280.3	4.412	0.0101	HOMO→LUMO+5 (3%)	
					HOMO→LUMO+2 (97%)	
	S <sub>4</sub>	261.8	4.723	0.0056	HOMO→LUMO+3 (61%)	
					HOMO→LUMO+4 (35%)	
	S <sub>5</sub>	253.3	4.883	0.003	HOMO→LUMO+4 (58%)	
					HOMO→LUMO+3 (32%)	
PBEh1PBE <sup>a</sup>	S <sub>1</sub>	351.1	3.523	0.0063	HOMO-1→LUMO (91%)	0.191
	S <sub>2</sub>	315.3	3.923	0.7332	HOMO-1→LUMO+2 (5%)	
					HOMO→LUMO (98%)	
	S <sub>3</sub>	230.7	5.361	0.0137	HOMO-1→LUMO (2%)	
					HOMO→LUMO+1 (97%)	
	S <sub>4</sub>	222.0	5.570	0.0063	HOMO-2→LUMO (53%)	
					HOMO→LUMO+2 (44%)	
PBEh1PBE (CH <sub>2</sub> Cl <sub>2</sub> ) <sup>b</sup>	S <sub>5</sub>	211.4	5.849	0.0049	HOMO-1→LUMO+2 (70%)	0.191
	S <sub>6</sub>	211.3	5.854	0.0093	HOMO-1→LUMO (6%)	
					HOMO→LUMO+4 (82%)	
	S <sub>1</sub>	351.5	3.518	0.8573	HOMO→LUMO+3 (10%)	
					HOMO→LUMO (99%)	
	S <sub>2</sub>	326.3	3.791	0.0079	HOMO-1→LUMO (93%)	
	S <sub>3</sub>	268.0	4.616	0.0139	HOMO→LUMO+1 (95%)	
PBEh1PBE (CH <sub>2</sub> Cl <sub>2</sub> ) <sup>b</sup>	S <sub>4</sub>	247.4	4.998	0.0103	HOMO→LUMO+5 (4%)	0.191
					HOMO→LUMO+2 (93%)	
	S <sub>5</sub>	243.3	5.084	0.0044	HOMO→LUMO+3 (76%)	
					HOMO→LUMO+4 (18%)	
	S <sub>6</sub>	237.7	5.204	0.0374	HOMO→LUMO+4 (72%)	
					HOMO→LUMO+3 (16%)	



Table 4. Cont.

 $\lambda_{\text{max,abs exp}} 373 \text{ nm}/3.327 \text{ eV } (71,000 \text{ M}^{-1} \text{ cm}^{-1})$						
Functional	State	$\lambda_{\text{max,abs calcd}}$		Oscillatory	Most Dominant	$\Delta E_{\text{calcd—exp}}$
		[nm]	[eV]	Strength $f$	Contribution (%)	[eV]
CAM-B3LYP <sup>a</sup>	S <sub>1</sub>	318.4	3.884	0.0261	HOMO-1→LUMO (78%) HOMO-1→LUMO+2 (6%)	0.775
	S <sub>2</sub>	301.5	4.102	0.6999	HOMO→LUMO (93%) HOMO-1→LUMO (5%)	
	S <sub>3</sub>	212.3	5.825	0.0179	HOMO→LUMO+1 (86%) HOMO→LUMO+6 (7%)	
	S <sub>4</sub>	204.2	6.058	0.0063	HOMO→LUMO+4 (69%) HOMO→LUMO+2 (11%)	
	S <sub>5</sub>	198.7	6.225	0.1157	HOMO-2→LUMO (86%) HOMO→LUMO+4 (6%)	
	S <sub>6</sub>	197.9	6.250	0.0379	HOMO→LUMO+2 (55%) HOMO→LUMO+3 (19%)	
CAM-B3LYP (CH <sub>2</sub> Cl <sub>2</sub> ) <sup>b</sup>	S <sub>1</sub>	343.2	3.604	0.8438	HOMO→LUMO (98%)	0.277
	S <sub>2</sub>	298.1	4.149	0.0024	HOMO-1→LUMO (80%) HOMO-1→LUMO+8 (4%)	
	S <sub>3</sub>	256.5	4.822	0.016	HOMO→LUMO+1 (77%) HOMO→LUMO+5 (12%)	
	S <sub>4</sub>	234.1	5.282	0.0084	HOMO→LUMO+3 (77%) HOMO→LUMO+9 (8%)	
	S <sub>5</sub>	229.0	5.401	0.0358	HOMO→LUMO+2 (48%) HOMO→LUMO+4 (21%)	
	S <sub>6</sub>	224.9	5.498	0.0206	HOMO→LUMO+4 (56%) HOMO→LUMO+2 (26%)	

<sup>a</sup> Gas phase calculation in absence of PCM. <sup>b</sup> Employing PCM for dichloromethane as a dielectric continuum. <sup>c</sup> Employing a state specific solvation for dichloromethane as a dielectric continuum.

**Table 5.** Experimentally determined longest wavelength absorption band (recorded in dichloromethane at  $T = 298 \text{ K}$ ) and TDDFT calculated absorption spectra of cyanine **6b** using various functionals and 6-311++G\*\* as a basis set.

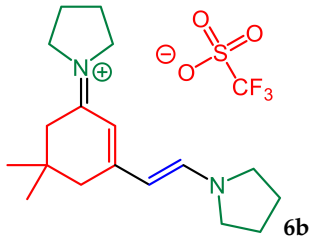
 $\lambda_{\text{max,abs exp}} 443 \text{ nm}/2.801 \text{ eV } (114,000 \text{ M}^{-1} \text{ cm}^{-1})$						
Functional	State	$\lambda_{\text{max,abs calcd}}$		Oscillatory	Most Dominant	$\Delta E_{\text{calcd—exp}}$
		[nm]	[eV]	Strength $f$	Contribution (%)	[eV]
B3LYP <sup>a</sup>	S <sub>1</sub>	362.2	3.415	0.9478	HOMO→LUMO (100%)	0.614
	S <sub>2</sub>	250.8	4.931	0.1102	HOMO-1→LUMO (76%) HOMO→LUMO+1 (22%)	
	S <sub>3</sub>	224.7	5.503	0.0268	HOMO-3→LUMO (55%) HOMO-2→LUMO (28%)	

Table 5. Cont.

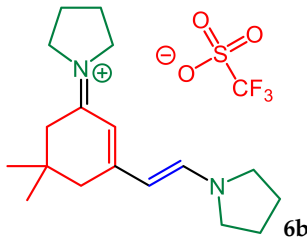
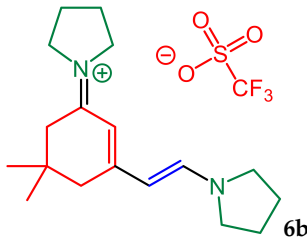
<div>  <div> <math>\lambda_{\text{max,abs exp}}</math> 443 nm/2.801 eV (114,000 M<sup>-1</sup>cm<sup>-1</sup>) </div> </div>						
Functional	State	$\lambda_{\text{max,abs calcd}}$		Oscillatory	Most Dominant	$\Delta E_{\text{calcd-exp}}$
		[nm]	[eV]	Strength $f$	Contribution (%)	[eV]
	S <sub>4</sub>	223.1	5.543	0.0803	HOMO→LUMO+1 (45%) HOMO-2→LUMO (34%)	
	S <sub>5</sub>	219.6	5.632	0.0075	HOMO→LUMO+2 (88%) HOMO→LUMO+4 (4%)	
	S <sub>6</sub>	215.7	5.734	0.0184	HOMO-4→LUMO (77%) HOMO-2→LUMO (12%)	
B3LYP (CH <sub>2</sub> Cl <sub>2</sub> ) <sup>b</sup>	S <sub>1</sub>	386.1	3.203	1.0034	HOMO→LUMO (100%)	0.402
	S <sub>2</sub>	261.3	4.734	0.0031	HOMO→LUMO+1 (95%)	
	S <sub>3</sub>	254.3	4.864	0.1198	HOMO-1→LUMO (61%) HOMO→LUMO+2 (35%)	
	S <sub>4</sub>	244.4	5.061	0.0263	HOMO→LUMO+3 (63%) HOMO→LUMO+2 (27%)	
	S <sub>5</sub>	239.2	5.171	0.036	HOMO→LUMO+4 (64%) HOMO→LUMO+2 (12%)	
	S <sub>6</sub>	233.7	5.292	0.1408	HOMO→LUMO+4 (26%) HOMO→LUMO+3 (22%)	
B3LYP (CH <sub>2</sub> Cl <sub>2</sub> ) <sup>c</sup>	S <sub>1</sub>	369.0	3.357	0.8976	HOMO→LUMO (100%)	0.556
	S <sub>2</sub>	261.2	4.735	0.0025	HOMO→LUMO+1 (95%)	
	S <sub>3</sub>	253.5	4.879	0.1085	HOMO-1→LUMO (57%) HOMO→LUMO+2 (39%)	
	S <sub>4</sub>	244.2	5.065	0.0193	HOMO→LUMO+3 (68%) HOMO→LUMO+2 (24%)	
	S <sub>5</sub>	239.2	5.170	0.0135	HOMO→LUMO+4 (76%) HOMO→LUMO+2 (6%)	
	S <sub>6</sub>	231.8	5.335	0.0975	HOMO→LUMO+2 (20%) HOMO→LUMO+3 (20%)	
PBEh1PBE <sup>a</sup>	S <sub>1</sub>	357.5	3.460	0.9557	HOMO→LUMO (100%)	0.659
	S <sub>2</sub>	242.7	5.096	0.1278	HOMO-1→LUMO (81%) HOMO→LUMO+1 (18%)	
	S <sub>3</sub>	219.4	5.638	0.0861	HOMO→LUMO+1 (45%) HOMO-3→LUMO (39%)	
	S <sub>4</sub>	218.0	5.673	0.0435	HOMO-2→LUMO (47%) HOMO→LUMO+1 (26%)	
	S <sub>5</sub>	210.5	5.875	0.0024	HOMO→LUMO+2 (88%) HOMO→LUMO+4 (5%)	
	S <sub>6</sub>	209.6	5.902	0.0174	HOMO-4→LUMO (79%) HOMO-2→LUMO (14%)	
PBEh1PBE (CH <sub>2</sub> Cl <sub>2</sub> ) <sup>b</sup>	S <sub>1</sub>	380.4	3.252	1.0153	HOMO→LUMO (99%)	0.451
	S <sub>2</sub>	250.2	4.944	0.0056	HOMO→LUMO+1 (93%)	
	S <sub>3</sub>	245.6	5.036	0.1362	HOMO-1→LUMO (66%) HOMO→LUMO+2 (30%)	
	S <sub>4</sub>	233.5	5.297	0.0846	HOMO→LUMO+2 (53%) HOMO→LUMO+3 (26%)	
	S <sub>5</sub>	230.7	5.360	0.0853	HOMO→LUMO+3 (49%) HOMO→LUMO+4 (23%)	

Table 5. Cont.



$\lambda_{\text{max,abs exp}} 443 \text{ nm}/2.801 \text{ eV} (114,000 \text{ M}^{-1}\text{cm}^{-1})$

Functional	State	$\lambda_{\text{max,abs calcd}}$ [nm]	[eV]	Oscillatory Strength $f$	Most Dominant Contribution (%)	$\Delta E_{\text{calcd-exp}}$ [eV]
	S <sub>6</sub>	226.5	5.461	0.0575	HOMO→LUMO+4 (65%) HOMO→LUMO+3 (18%)	
CAM-B3LYP <sup>a</sup>	S <sub>1</sub>	354.7	3.487	0.9695	HOMO→LUMO (98%)	0.686
	S <sub>2</sub>	220.5	5.610	0.2421	HOMO-1→LUMO (94%)	
	S <sub>3</sub>	209.1	5.914	0.0763	HOMO→LUMO+1 (96%)	
	S <sub>4</sub>	202.9	6.096	0.003	HOMO→LUMO+2 (73%)	
	S <sub>5</sub>	201.0	6.152	0.0013	HOMO→LUMO+4 (14%)	
	S <sub>6</sub>	189.3	6.535	0.0022	HOMO-3→LUMO (49%) HOMO-2→LUMO (35%) HOMO-4→LUMO (83%) HOMO-3→LUMO (3%)	
CAM-B3LYP (CH <sub>2</sub> Cl <sub>2</sub> ) <sup>b</sup>	S <sub>1</sub>	377.4	3.277	1.0218	HOMO→LUMO (98%) HOMO→LUMO+1 (78%)	0.476
	S <sub>2</sub>	239.9	5.155	0.0013	HOMO→LUMO+5 (7%)	
	S <sub>3</sub>	226.3	5.465	0.2191	HOMO-1→LUMO (30%) HOMO→LUMO+4 (17%)	
	S <sub>4</sub>	221.5	5.584	0.1968	HOMO-1→LUMO (64%) HOMO→LUMO+4 (9%)	
	S <sub>5</sub>	219.7	5.630	0.0256	HOMO→LUMO+3 (45%) HOMO→LUMO+2 (25%)	
	S <sub>6</sub>	213.9	5.781	0.0197	HOMO→LUMO+2 (38%) HOMO→LUMO+3 (16%)	

<sup>a</sup> Gas phase calculation in absence of PCM. <sup>b</sup> Employing PCM for dichloromethane as a dielectric continuum. <sup>c</sup> Employing a state specific solvation for dichloromethane as a dielectric continuum.

For merocyanine **5b**, the longest wavelength band apparently depends on solvent stabilization (Table 4). While gas phase calculations with B3LYP, PBEh1PBE, and CAM-B3LYP functionals predict lowest energy bands of weak intensity dominated by an n- $\pi^*$  (HOMO-1→LUMO) transition as singlet S<sub>1</sub> state, the highest intensity  $\pi$ - $\pi^*$  (HOMO→LUMO) transition represents the S<sub>2</sub> state. The solvation effect becomes apparent for all functionals upon employing the implicit PCM for dichloromethane as a continuum, which was actually also used in experimental spectroscopy. For PCM calculations, the lowest energy, highest intensity band predominantly consists of  $\pi$ - $\pi^*$  (HOMO→LUMO) transition, yet, with a minor contribution of the n- $\pi^*$  (HOMO-1→LUMO) transition in singlet S<sub>1</sub> state as shown for the B3LYP with state specific solvation. As seen for all merocyanines **5**, emission cannot be detected by the naked eye nor with steady state fluorescence spectroscopy (vide supra).

All TDDFT calculations on merocyanine **5b** give higher energies for the lowest energy band than the experimentally determined values by 0.127 to 0.775 eV. Indeed, the smallest deviations are found for the functionals B3LYP (0.127 eV) and PBEh1PBE (0.191 eV) with explicit PCM implementation. These deviations fall into the same range as previously reported for TDDFT calculations on cyanines [45]. The Kohn-Sham frontier molecular orbitals of the B3LYP/6-311++G\*\* PCM calculations nicely illustrate that the intense longest wavelength absorption is dominated by HOMO→LUMO transition along the chromophore axis (Figure 6, left). The less dominant, weak intensely HOMO-1→LUMO transition clearly

possesses  $n\text{-}\pi^*$  character. In the experiment, this transition might fall in superposition with the broad intense merocyanine  $\pi\text{-}\pi^*$  band.

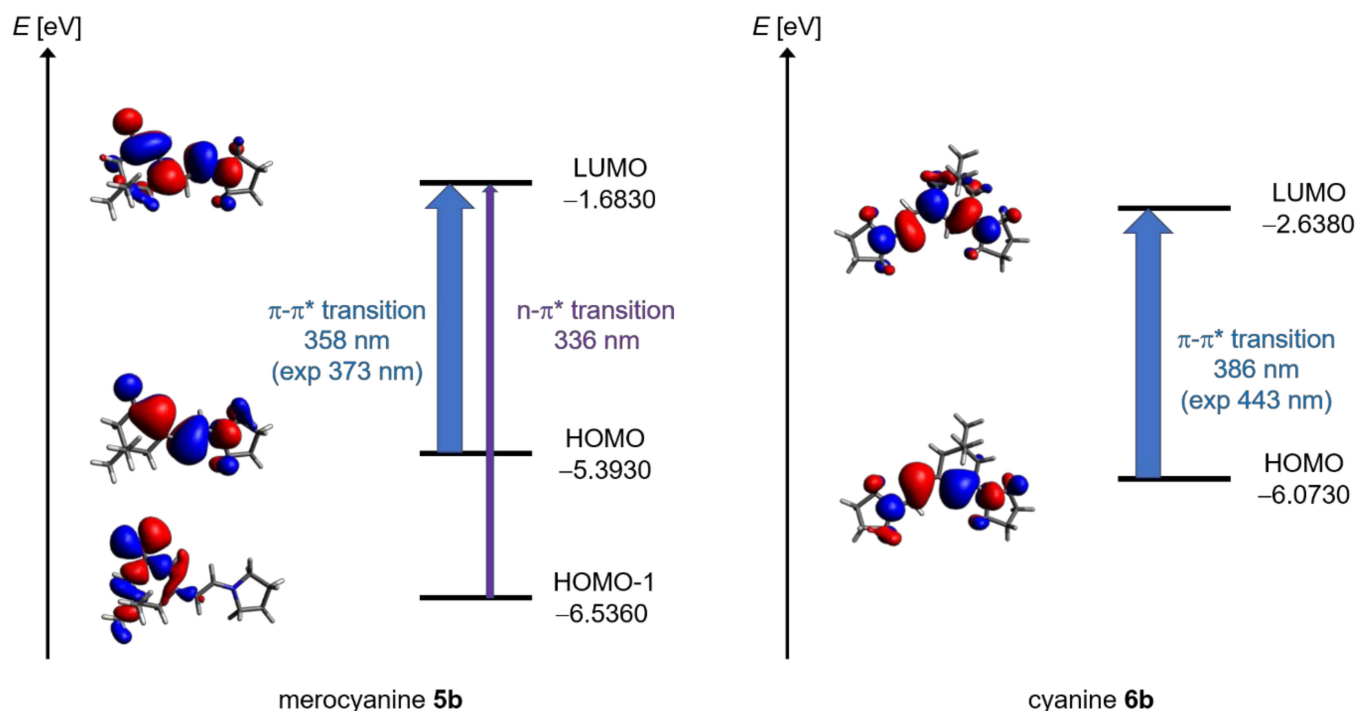


**Figure 6.** Selected Kohn-Sham frontier molecular orbitals of merocyanine **5b** (left) and cyanine **6b** (right) (Gaussian 16 B3LYP/6-311++G\*\*, PCM  $\text{CH}_2\text{Cl}_2$ , isosurface value at 0.04) and the calculated HOMO, HOMO-1, and LUMO energies, including the energy differences between the frontier molecular orbitals as well as the calculated and experimentally determined absorption wavelength of merocyanine **5b** and cyanine **6b**.

Expectedly for cyanine **6b**, the PCM solvent implementation predicts the absorption to arise at longer wavelengths in comparison to the gas phase calculations (Table 5). For all exchange correlation hybrid functionals the lowest energy transition is fully represented by HOMO $\rightarrow$ LUMO transition along the cyanine chromophore axis, as also seen in the Kohn-Sham frontier molecular orbitals (Figure 6, right). As stated above and typical for cyanines, the calculated transition energies for this band are higher and deviate by 0.402 to 0.686 eV in comparison to the experimentally determined absorption energy. As mentioned before, the functionals B3LYP (0.402 eV) and PBEh1PBE (0.451 eV) with explicit PCM implementation possess the smallest deviations.

### 3. Conclusions

The triflate readily accessible from dimedone is a favorable starting material for consecutive three-component alkynylation-addition sequences to merocyanines with embedded butadiene structure in moderate to excellent yield. Moreover, employing pyrrolidine as an amino component enables a pseudo four-component synthesis of related cyanines by carbonyl condensation of the heterocyclic amine in excellent yield. While butadiene-based (absorption between 360 and 390 nm) and expanded hexatriene (absorption at 442 nm) chromophores are essentially nonfluorescent in solution and in the solid state, the pentamethine cyanines absorb intensively at 443 and 459 nm and also luminesce in solution with low fluorescence quantum yield of 1%. According to TDDFT calculations with various exchange correlation hybrid functionals in the gas phase and in an explicit continuum of dichloromethane, the electronic structure of the longest wavelength absorption bands is highly solvent dependent for both a representative merocyanine and a cyanine. The cyanine typical deviation of calculated transitions to higher energies in comparison to

the experimental data falls in a regime of 0.127 eV for the merocyanine and 0.402 eV for the model cyanine. For merocyanines, the lowest energy absorption band contains  $n-\pi^*$  character, which plausibly accounts for the indiscernible luminescence. In contrast, the rigidified cyanine's lowest energy band is exclusively a  $\pi-\pi^*$  transition and does not interfere with luminescence. The synthetic ease of accessing both merocyanines and cyanines in a one-pot fashion allows for readily preparing substance libraries of both chromophore types, which can be interesting for biophysical analytics. Studies directed to expand the one-pot methodology to bathochromically shifted merocyanines based upon the dimedone derived triflate are currently underway.

#### 4. Experimental

##### 4.1. 5,5-Dimethyl-3-oxocyclohex-1-en-1-yl trifluoromethanesulfonate (2)

In a Schlenk flask with magnetic stir bar, dimedone (**1**) (2.80 g, 20.0 mmol) was dissolved in dichloromethane (50 mL) under nitrogen and the solution was cooled to 0 °C (ice water bath) before pyridine (2.00 mL, 24.8 mmol) was added. Trifluoromethanesulfonic anhydride (3.90 mL, 23.2 mmol) was added dropwise to the cooled solution over a period of 1 h. The cooling was stopped and the reaction mixture was stirred at room temp for 2 h. Then, a 1 M aqueous HCl solution (25 mL) was added. The organic layer was washed with a saturated aqueous NaHCO<sub>3</sub> solution (3 × 20 mL) and dried (anhydrous Na<sub>2</sub>SO<sub>4</sub>). After filtration and removal of the solvents in vacuo, the crude product was purified by flash chromatography on silica gel (*n*-hexane/ethyl acetate 98:2) to give compound **1** [34] (4.94 g, 91%) as a pale-yellow liquid, *R<sub>f</sub>* (*n*-hexane/ethyl acetate 20:1): 0.14.

<sup>1</sup>H NMR (600 MHz, CDCl<sub>3</sub>):  $\delta$  1.13 (s, 6 H), 2.30 (s, 2 H), 2.54 (d, *J* = 1.3 Hz, 2 H), 6.06 (t, *J* = 1.3 Hz, 1 H). <sup>13</sup>C NMR (151 MHz, CDCl<sub>3</sub>):  $\delta$  28.1 (CH<sub>3</sub>), 33.5 (C<sub>quat</sub>), 42.4 (CH<sub>2</sub>), 50.6 (CH<sub>2</sub>), 118.4 (CH), 118.5 (C<sub>quat</sub>, q, <sup>1</sup>*J*<sub>C-F</sub> = 321 Hz), 166.1 (C<sub>quat</sub>), 197.6 (C<sub>quat</sub>). EI MS (70 eV, *m/z* (%)): 272 (18, [M<sup>+</sup>]), 244 (15, [C<sub>8</sub>H<sub>11</sub>O<sub>3</sub>SF<sub>3</sub><sup>+</sup>]), 216 (100), 86 (28), 83 (16), 69 (38, [CF<sub>3</sub><sup>+</sup>]), 56 (10), 55 (11), 41 (12).

##### 4.2. General Procedure (GP) for the Three-Component Synthesis of Merocyanines 5 and 8

PdCl<sub>2</sub>(PPh<sub>3</sub>)<sub>2</sub> (14 mg, 0.02 mmol), CuI (7 mg, 0.04 mmol), compound **2** (272 mg, 1.00 mmol), and dry, degassed THF (1 mL) were placed in a microwave vessel. The solution was saturated with a constant stream of nitrogen through a syringe for 5 min. Then, alkyne **3** (1.0 mmol), K<sub>2</sub>CO<sub>3</sub> (166 mg, 1.20 mmol), or triethylamine (0.14 mL, 1.00 mmol) were added and the mixture was stirred at room temp for 1 h (for experimental details, see Table 6). Then, the amine **4** or Fischer's base (**7**) (1.0 mmol) and methanol (1 mL) were added to the reaction mixture. The reaction mixture was then heated in the microwave cavity at 100 °C for 1 h. After cooling to room temp, the solvents were removed under reduced pressure and the residue was purified by flash chromatography on silica gel (*n*-hexane/ethyl acetate) to give the analytically pure product merocyanine **5** and **8**.

**Table 6.** Experimental details of the consecutive three-component synthesis of merocyanines **5** and **8** with potassium carbonate as a base.

Entry	Alkyne 3	Amine 4 or Fischer's Base (7)	Yield of Merocyanines 5 and 8
1 <sup>a</sup>	140 $\mu$ L (1.00 mmol) of <b>3a</b>	90 $\mu$ L (1.0 mmol) of <b>4a</b>	135 mg (65%) of <b>5a</b>
2 <sup>b</sup>	140 $\mu$ L (1.00 mmol) of <b>3a</b>	90 $\mu$ L (1.0 mmol) of <b>4a</b>	82 mg (35%) of <b>5a</b>
3 <sup>a</sup>	140 $\mu$ L (1.00 mmol) of <b>3a</b>	85 $\mu$ L (1.0 mmol) of <b>4c</b>	71 mg (53%) of <b>5b</b>
4 <sup>a</sup>	110 $\mu$ L (1.00 mmol) of <b>3d</b>	90 $\mu$ L (1.0 mmol) of <b>4a</b>	171 mg (55%) of <b>5c</b>
5 <sup>b</sup>	110 $\mu$ L (1.00 mmol) of <b>3d</b>	90 $\mu$ L (1.0 mmol) of <b>4a</b>	212 mg (68%) of <b>5c</b>
6 <sup>a</sup>	110 $\mu$ L (1.00 mmol) of <b>3d</b>	100 $\mu$ L (1.00 mmol) of <b>4b</b>	191 mg (62%) of <b>5d</b>
7 <sup>b</sup>	110 $\mu$ L (1.00 mmol) of <b>3d</b>	100 $\mu$ L (1.00 mmol) of <b>4b</b>	62 mg (20%) of <b>5d</b>
8 <sup>a</sup>	110 $\mu$ L (1.00 mmol) of <b>3d</b>	85 $\mu$ L (1.0 mmol) of <b>4c</b>	118 mg (40%) of <b>5e</b>
9 <sup>b</sup>	140 $\mu$ L (1.00 mmol) of <b>3a</b>	180 $\mu$ L (1.00 mmol) of 1,3,3-trimethyl-2-methylenindoline ( <b>7</b> )	21 mg (7%) of <b>8</b>

<sup>a</sup> The reaction was performed with K<sub>2</sub>CO<sub>3</sub> as a base. <sup>b</sup> The reaction was performed with NEt<sub>3</sub> as a base.

#### 4.3. (E)-5,5-Dimethyl-3-(2-morpholinovinyl)cyclohex-2-en-1-one (5a)

According to the GP and after chromatography on silica gel (*n*-hexane/ethyl acetate 2:1) and drying under vacuum, compound **5a** (135 mg, 65%, with potassium carbonate as a base; 82 mg, 35%, with triethylamine as a base) was obtained as an orange solid, mp 72 °C, *R<sub>f</sub>* (*n*-hexane/ethyl acetate 2:1): 0.12.

<sup>1</sup>H NMR (600 MHz, MeOD-*d*<sub>4</sub>): δ 1.08 (s, 6 H), 2.22 (s, 2 H), 2.43 (s, 2 H), 3.34 (t, *J* = 4.7 Hz, 4 H), 3.73 (t, *J* = 4.9 Hz, 4 H), 5.43 (d, *J* = 13.5 Hz, 1 H), 5.71 (s, 1 H), 7.15 (d, *J* = 13.5 Hz, 1 H). <sup>13</sup>C NMR (151 MHz, MeOD-*d*<sub>4</sub>): δ 28.5 (CH<sub>3</sub>), 34.0 (C<sub>quat</sub>), 40.2 (CH<sub>2</sub>), 49.7 (CH<sub>2</sub>), 51.4 (CH<sub>2</sub>), 67.2 (CH<sub>2</sub>), 100.4 (CH), 116.3 (CH), 148.0 (CH), 164.4 (C<sub>quat</sub>), 200.9 (C<sub>quat</sub>). EI MS (70 eV, *m/z* (%)): 236 (18), 235 (100, [M<sup>+</sup>]), 222 (10), 221 (11), 220 (31, [C<sub>13</sub>H<sub>18</sub>NO<sub>2</sub><sup>+</sup>]), 214 (15), 207 (19, [C<sub>12</sub>H<sub>17</sub>NO<sub>2</sub><sup>+</sup>]), 206 (16), 192 (22), 179 (13, [C<sub>10</sub>H<sub>13</sub>NO<sub>2</sub><sup>+</sup>]), 178 (31), 153 (12), 152 (13), 151 (15, [C<sub>9</sub>H<sub>13</sub>NO<sup>+</sup>]), 150 (18), 149 (20, [C<sub>10</sub>H<sub>13</sub>O<sup>+</sup>]), 138 (19, [C<sub>8</sub>H<sub>12</sub>NO<sup>+</sup>]), 136 (48, [C<sub>9</sub>H<sub>12</sub>O<sup>+</sup>]), 135 (11), 122 (20), 121 (41), 120 (13), 112 (12, [C<sub>6</sub>H<sub>10</sub>NO<sup>+</sup>]), 107 (16), 106 (11), 105 (15), 100 (11), 94 (17), 93 (56), 91 (11), 86 (17, [C<sub>4</sub>H<sub>8</sub>NO<sup>+</sup>]), 85 (20), 79 (14), 77 (14), 67 (14), 65 (12), 57 (10), 56 (14), 55 (21), 42 (10), 41 (13). IR:  $\tilde{\nu}$  [cm<sup>-1</sup>]: 3053 (w), 3026 (w), 2955 (w), 2926 (w), 2891 (w), 2864 (w), 1589 (s), 1553 (s), 1504 (w), 1443 (m), 1422 (m), 1412 (m), 1375 (m), 1319 (m), 1298 (m), 1277 (s), 1252 (m), 1227 (m), 1194 (m), 1152 (m), 1109 (s), 1069 (m), 1047 (w), 1020 (m), 995 (m), 943 (m), 924 (w), 854 (m), 822 (w), 799 (w), 756 (w), 745 (w), 725 (w), 681 (m), 602 (m). Anal calcd for C<sub>14</sub>H<sub>21</sub>NO<sub>2</sub> (235.3): C 71.46, H 8.99, N 5.95; Found: C 71.27, H 9.28, N 5.93.

#### 4.4. (E)-5,5-Dimethyl-3-[2-(pyrrolidin-1-yl)vinyl]cyclohex-2-en-1-one (5b)

According to the GP and after chromatography on silica gel (*n*-hexane/ethyl acetate 3:1) and drying under vacuum, compound **5b** (116 mg, 53%) was obtained as a yellow solid, mp 125 °C, *R<sub>f</sub>* (*n*-hexane/ethyl acetate/NEt<sub>3</sub> 200:100:3): 0.14.

<sup>1</sup>H NMR (600 MHz, CDCl<sub>3</sub>): δ 1.04 (s, 6 H), 1.94 (t, *J* = 6.6 Hz, 4 H), 2.20 (s, 2 H), 2.27 (s, 2 H), 3.30 (t, *J* = 6.7 Hz, 4 H), 5.04 (d, *J* = 13.4 Hz, 1 H), 5.70 (s, 1 H), 7.08 (d, *J* = 13.3 Hz, 1 H). <sup>13</sup>C NMR (151 MHz, CDCl<sub>3</sub>): δ 25.1 (CH<sub>2</sub>), 28.5 (CH<sub>3</sub>), 33.0 (C<sub>quat</sub>), 39.6 (CH<sub>2</sub>), 49.1 (CH<sub>2</sub>), 50.9 (CH<sub>2</sub>), 99.2 (CH), 116.2 (CH), 141.4 (CH), 158.9 (C<sub>quat</sub>), 198.3 (C<sub>quat</sub>). EI MS (70 eV, *m/z* (%)): 220 (19), 219 (100, [M<sup>+</sup>]), 204 (55, [C<sub>13</sub>H<sub>18</sub>NO<sup>+</sup>]), 191 (11, [C<sub>12</sub>H<sub>17</sub>NO<sup>+</sup>]), 190 (16), 176 (23), 163 (10, [C<sub>10</sub>H<sub>13</sub>NO<sup>+</sup>]), 162 (20), 136 (17, [C<sub>9</sub>H<sub>12</sub>O<sup>+</sup>]), 135 (42, [C<sub>9</sub>H<sub>13</sub>N<sup>+</sup>]), 134 (86), 122 (13, [C<sub>8</sub>H<sub>12</sub>N<sup>+</sup>]), 121 (10), 120 (43), 107 (59), 106 (16), 93 (12), 79 (11), 70 (10, [C<sub>4</sub>H<sub>8</sub>N<sup>+</sup>]). IR:  $\tilde{\nu}$  [cm<sup>-1</sup>]: 3051 (w), 3013 (w), 2990 (w), 2955 (w), 2926 (w), 2857 (w), 1636 (w), 1585 (s), 1560 (s), 1550 (s), 1545 (s), 1533 (m), 1481 (m), 1459 (w), 1452 (w), 1406 (m), 1383 (s), 1369 (s), 1358 (s), 1315 (m), 1306 (m), 1292 (m), 1275 (s), 1248 (s), 1194 (m), 1161 (m), 1148 (s), 1119 (s), 1032 (w), 1018 (w), 980 (m), 924 (w), 912 (w), 891 (m), 866 (m), 847 (s), 806 (w), 791 (m), 704 (w), 606 (m). UV/Vis (CH<sub>2</sub>Cl<sub>2</sub>): λ<sub>max</sub> [nm] (ε [Lcm<sup>-1</sup>mol<sup>-1</sup>]): 373 (71000). Anal calcd for C<sub>14</sub>H<sub>21</sub>NO (219.3): C 76.67, H 9.65, N 6.39; Found: C 76.43, H 9.94, N 6.17.

#### 4.5. (E)-5,5-Dimethyl-3-(2-morpholino-2-phenylvinyl)cyclohex-2-en-1-one (5c)

According to the GP and after chromatography on silica gel (*n*-hexane/ethyl acetate 3:1) and drying under vacuum, compound **5c** (171 mg, 55%, with potassium carbonate as a base; 212 mg, 68%, with triethylamine as a base) was obtained as a yellow solid, mp 78 °C, *R<sub>f</sub>* (*n*-hexane/ethyl acetate 3:1): 0.09.

<sup>1</sup>H NMR (600 MHz, DMSO-*d*<sub>6</sub>): δ 0.76 (s, 6 H), 1.75 (s, 2 H), 1.92 (s, 2 H), 2.94 (t, *J* = 4.8 Hz, 4 H), 3.60 (t, *J* = 4.8 Hz, 4 H), 5.30 (s, 1 H), 5.28 (s, 1 H), 7.16–7.32 (m, 2 H), 7.37–7.48 (m, 3 H). <sup>13</sup>C NMR (151 MHz, DMSO-*d*<sub>6</sub>): δ 27.8 (CH<sub>3</sub>), 32.9 (C<sub>quat</sub>), 43.4 (CH<sub>2</sub>), 48.3 (CH<sub>2</sub>), 50.3 (CH<sub>2</sub>), 65.8 (CH<sub>2</sub>), 103.9 (CH), 121.1 (CH), 128.8 (CH), 129.3 (CH), 129.4 (CH), 136.4 (C<sub>quat</sub>), 156.2 (C<sub>quat</sub>), 157.9 (C<sub>quat</sub>), 196.9 (C<sub>quat</sub>). EI MS (70 eV, *m/z* (%)): 312 (22), 311 (100, [M<sup>+</sup>]), 310 (26), 296 (11, [C<sub>19</sub>H<sub>22</sub>NO<sub>2</sub><sup>+</sup>]), 295 (17), 294 (76), 254 (19), 252 (11), 227 (14, [C<sub>15</sub>H<sub>17</sub>NO<sup>+</sup>]), 226 (13), 225 (21, [C<sub>16</sub>H<sub>17</sub>O<sup>+</sup>]), 212 (32), 198 (11), 196 (12), 170 (11), 169 (14), 168 (15), 141 (15), 105 (60), 77 (17, [C<sub>6</sub>H<sub>5</sub><sup>+</sup>]), 43 (11). IR:  $\tilde{\nu}$  [cm<sup>-1</sup>]: 3030 (w), 2963 (w), 2932 (w), 2913 (w), 2899 (w), 2855 (w), 2822 (w), 1639 (m), 1579 (m), 1570 (s),



1557 (m), 1539 (m), 1489 (w), 1443 (m), 1437 (w), 1387 (m), 1358 (m), 1314 (w), 1298 (m), 1281 (m), 1267 (m), 1248 (w), 1225 (s), 1214 (m), 1204 (s), 1175 (w), 1148 (w), 1111 (s), 1077 (w), 1069 (m), 1030 (m), 1020 (m), 999 (w), 941 (w), 932 (m), 903 (w), 889 (m), 883 (m), 862 (m), 849 (m), 808 (w), 777 (s), 735 (m), 710 (m), 692 (m), 644 (w), 623 (m). UV/Vis (CH<sub>2</sub>Cl<sub>2</sub>):  $\lambda_{\max}$  [nm] ( $\epsilon$  [Lcm<sup>-1</sup>mol<sup>-1</sup>]): 365 (19000). Anal calcd for C<sub>20</sub>H<sub>25</sub>NO<sub>2</sub> (311.4): C 77.14, H 8.09, N 4.50; Found: C 76.90, H 8.33, N 4.34.

#### 4.6. (E)-5,5-Dimethyl-3-[2-phenyl-2-(piperidin-1-yl)vinyl]cyclohex-2-en-1-one (5d)

According to the GP and after chromatography on silica gel (*n*-hexane/ethyl acetate/NEt<sub>3</sub> 500:100:6) and drying under vacuum, compound **5d** (191 mg, 62%, with potassium carbonate as a base; 62 mg, 20%, with triethylamine as a base) was obtained as an orange solid, mp 86 °C, *R<sub>f</sub>* (*n*-hexane/ethyl acetate/NEt<sub>3</sub> 500:100:6): 0.08.

<sup>1</sup>H NMR (600 MHz, CDCl<sub>3</sub>):  $\delta$  0.80 (s, 6 H), 1.53–1.56 (m, 2 H), 1.56–1.63 (m, 4 H), 1.68 (s, 2 H), 2.03 (s, 2 H), 3.02 (t, *J* = 5.2 Hz, 4 H), 5.23 (s, 1 H), 5.48 (s, 1 H), 7.23–7.25 (m, 2 H), 7.33–7.42 (m, 3 H). <sup>13</sup>C NMR (151 MHz, CDCl<sub>3</sub>):  $\delta$  24.5 (CH<sub>2</sub>), 25.9 (CH<sub>2</sub>), 28.2 (CH<sub>3</sub>), 33.5 (C<sub>quat</sub>), 44.1 (CH<sub>2</sub>), 49.7 (CH<sub>2</sub>), 50.9 (CH<sub>2</sub>), 104.1 (CH), 121.3 (CH), 128.7 (CH), 129.3 (CH), 129.7 (CH), 137.6 (C<sub>quat</sub>), 157.7 (C<sub>quat</sub>), 159.9 (C<sub>quat</sub>), 199.0 (C<sub>quat</sub>). EI MS (70 eV, *m/z* (%)): 310 (15), 309 (68, [M<sup>+</sup>]), 308 (28), 294 (10, [C<sub>20</sub>H<sub>24</sub>NO<sup>+</sup>]), 293 (16), 292 (68), 280 (11, [C<sub>19</sub>H<sub>21</sub>NO<sup>+</sup>]), 253 (10, [C<sub>17</sub>H<sub>19</sub>NO<sup>+</sup>]), 252 (41), 225 (19, [C<sub>16</sub>H<sub>17</sub>O<sup>+</sup>]), 224 (29), 211 (20), 210 (100, [C<sub>15</sub>H<sub>14</sub>O<sup>+</sup>]), 196 (10), 170 (13), 141 (15), 115 (11), 105 (12), 104 (10), 84 (14, [C<sub>5</sub>H<sub>10</sub>N<sup>+</sup>]). IR:  $\tilde{\nu}$  [cm<sup>-1</sup>]: 2988 (w), 2936 (w), 2864 (w), 2828 (w), 1628 (m), 1576 (w), 1561 (m), 1551 (s), 1546 (s), 1541 (s), 1534 (s), 1522 (m), 1518 (m), 1508 (m), 1491 (w), 1462 (w), 1449 (m), 1441 (m), 1420 (w), 1370 (m), 1364 (m), 1302 (m), 1279 (m), 1263 (w), 1227 (s), 1202 (m), 1157 (w), 1138 (m), 1119 (m), 1101 (s), 1070 (w), 1028 (w), 1007 (w), 918 (w), 895 (m), 880 (m), 860 (m), 851 (m), 831 (m), 818 (w), 797 (w), 777 (s), 725 (m), 702 (m), 675 (m), 638 (w), 606 (m). UV/Vis (CH<sub>2</sub>Cl<sub>2</sub>):  $\lambda_{\max}$  [nm] ( $\epsilon$  [Lcm<sup>-1</sup>mol<sup>-1</sup>]): 383 (22000). HRMS (ESI, *m/z* (%)) calcd for [C<sub>21</sub>H<sub>28</sub>NO]<sup>+</sup>: 310.2165 (100), 311.2199 (23), 312.2233 (3); Found: 310.2170 (100), 311.2201 (19), 312.2231 (3).

#### 4.7. (E)-5,5-Dimethyl-3-[2-phenyl-2-(pyrrolidin-1-yl)vinyl]cyclohex-2-en-1-one (5e)

According to the GP and after chromatography on silica gel (*n*-hexane/ethyl acetate/NEt<sub>3</sub> 200:100:3) and drying under vacuum, compound **5e** (118 mg, 40%) was obtained as an orange solid, mp 133 °C, *R<sub>f</sub>* (*n*-hexane/ethyl acetate/NEt<sub>3</sub> 200:100:3): 0.17.

<sup>1</sup>H NMR (600 MHz, CDCl<sub>3</sub>):  $\delta$  0.78 (s, 6 H), 1.65 (s, 2 H), 1.89 (t, *J* = 6.7 Hz, 4 H), 2.01 (s, 2 H), 3.15 (t, *J* = 6.3 Hz, 4 H), 5.05 (s, 1 H), 5.41 (s, 1 H), 7.19–7.25 (m, 2 H), 7.35–7.47 (m, 3 H). <sup>13</sup>C NMR (151 MHz, CDCl<sub>3</sub>):  $\delta$  25.4 (CH<sub>2</sub>), 28.3 (CH<sub>3</sub>), 33.2 (C<sub>quat</sub>), 44.0 (CH<sub>2</sub>), 49.2 (CH<sub>2</sub>), 50.7 (CH<sub>2</sub>), 100.2 (CH), 118.4 (CH), 128.6 (CH), 128.9 (CH), 129.0 (CH), 137.9 (C<sub>quat</sub>), 154.9 (C<sub>quat</sub>), 159.8 (C<sub>quat</sub>), 198.6 (C<sub>quat</sub>). EI MS (70 eV, *m/z* (%)): 296 (15), 295 (73, [M<sup>+</sup>]), 294 (24), 280 (34, [C<sub>19</sub>H<sub>22</sub>NO<sup>+</sup>]), 279 (21), 278 (94), 239 (11, [C<sub>16</sub>H<sub>17</sub>NO<sup>+</sup>]), 238 (32), 211 (18, [C<sub>15</sub>H<sub>17</sub>N<sup>+</sup>]), 210 (31), 197 (21, [C<sub>14</sub>H<sub>15</sub>N<sup>+</sup>]), 196 (100), 183 (10), 182 (15), 170 (12), 168 (11), 167 (10), 142 (10), 141 (17), 115 (13), 105 (11). IR:  $\tilde{\nu}$  [cm<sup>-1</sup>]: 3057 (w), 2945 (w), 2978 (w), 2864 (w), 2843 (w), 1620 (m), 1533 (s), 1501 (m), 1474 (m), 1453 (m), 1445 (m), 1425 (m), 1366 (s), 1344 (m), 1315 (m), 1302 (s), 1279 (s), 1254 (m), 1229 (m), 1204 (s), 1179 (m), 1165 (m), 1140 (s), 1109 (s), 1074 (m), 1028 (w), 991 (m), 970 (w), 937 (w), 924 (m), 893 (m), 885 (m), 876 (s), 864 (m), 804 (w), 775 (s), 743 (w), 706 (s), 691 (m), 673 (w), 631 (w). UV/Vis (CH<sub>2</sub>Cl<sub>2</sub>):  $\lambda_{\max}$  [nm] ( $\epsilon$  [Lcm<sup>-1</sup>mol<sup>-1</sup>]): 388 (43000). Anal calcd for C<sub>20</sub>H<sub>25</sub>NO (295.4): C 81.31, H 8.53, N 4.74; Found: C 81.02, H 8.80, N 4.58.

#### 4.8. 5,5-Dimethyl-3-[(E)-3-((E)-1,3,3-trimethylindolin-2-yliden)prop-1-en-1-yl]cyclohex-2-en-1-one (8)

According to the GP and after chromatography on silica gel (*n*-hexane/ethyl acetate/NEt<sub>3</sub> 300:100:4) and drying under vacuum, compound **8** (21 mg, 7%) was obtained as an orange solid, mp 86 °C, *R<sub>f</sub>* (*n*-hexane/ethyl acetate/NEt<sub>3</sub> 300:100:4): 0.31.

$^1\text{H}$  NMR (600 MHz,  $\text{CDCl}_3$ ):  $\delta$  1.10 (s, 6 H), 1.61 (s, 6 H), 2.27 (s, 2 H), 2.39 (s, 2 H), 3.15 (s, 3 H), 5.42 (d,  $J$  = 12.0 Hz, 1 H), 5.90 (s, 1 H), 6.11 (d,  $J$  = 14.6 Hz, 1 H), 6.66 (d,  $^3J$  = 7.8 Hz, 1 H), 6.89 (t,  $J$  = 7.4 Hz, 1 H), 7.13–7.21 (m, 2 H), 7.30 (dd,  $J$  = 14.8, 12.0 Hz, 1 H).  $^{13}\text{C}$  NMR (151 MHz,  $\text{CDCl}_3$ ):  $\delta$  28.7 ( $\text{CH}_3$ ), 28.8 ( $\text{CH}_3$ ), 29.3 ( $\text{CH}_3$ ), 33.4 ( $\text{C}_{\text{quat}}$ ), 39.7 ( $\text{CH}_2$ ), 46.1 ( $\text{C}_{\text{quat}}$ ), 51.5 ( $\text{CH}_2$ ), 96.5 ( $\text{CH}$ ), 106.6 ( $\text{CH}$ ), 120.4 ( $\text{CH}$ ), 121.7 ( $\text{CH}$ ), 122.3 ( $\text{CH}$ ), 124.6 ( $\text{CH}$ ), 128.0 ( $\text{CH}$ ), 132.9 ( $\text{CH}$ ), 138.9 ( $\text{C}_{\text{quat}}$ ), 144.8 ( $\text{C}_{\text{quat}}$ ), 156.9 ( $\text{C}_{\text{quat}}$ ), 160.8 ( $\text{C}_{\text{quat}}$ ), 199.9 ( $\text{C}_{\text{quat}}$ ). IR:  $\tilde{\nu}$  [ $\text{cm}^{-1}$ ]: 3049 (w), 2955 (w), 2924 (w), 2864 (w), 1641 (w), 1618 (m), 1595 (m), 1576 (m), 1541 (s), 1537 (s), 1489 (m), 1456 (m), 1375 (m), 1364 (m), 1350 (m), 1339 (m), 1314 (m), 1300 (m), 1273 (s), 1246 (m), 1204 (m), 1182 (m), 1165 (m), 1148 (s), 1115 (s), 1078 (m), 1042 (w), 1030 (w), 1020 (m), 993 (w), 959 (m), 930 (m), 897 (w), 878 (m), 858 (m), 831 (w), 806 (m), 797 (m), 741 (s), 716 (w), 656 (w), 637 (w), 604 (w). UV/Vis ( $\text{CH}_2\text{Cl}_2$ ):  $\lambda_{\text{max}}$  [nm] ( $\epsilon$  [ $\text{Lcm}^{-1}\text{mol}^{-1}$ ]): 275 (14000), 442 (27000). HRMS (ESI) calcd for  $[\text{C}_{22}\text{H}_{28}\text{NO}]^+$ : 322.2165 (100), 323.2199 (24), 324.2233 (3); Found: 322.2169 (100), 323.2203 (23), 324.2233 (3).

#### 4.9. General Procedure (GP) for the Pseudo Four-Component Synthesis of Cyanines 6

$\text{PdCl}_2(\text{PPh}_3)_2$  (14 mg, 0.02 mmol),  $\text{CuI}$  (7 mg, 0.04 mmol), compound **13** (272 mg, 1.00 mmol), and dry, degassed THF (1 mL) were placed in a microwave vessel. The solution was saturated with a constant stream of nitrogen through a syringe for 5 min. Then, alkyne **7** (1.0 mmol) and triethylamine (0.14 mL, 1.00 mmol) were added and the mixture was stirred at room temp for 1 h (for experimental details, see Table 7). Then, the pyrrolidine (**9c**) (1.0 mmol) and methanol (1 mL) were added to the reaction mixture. The reaction mixture was then heated in the microwave cavity at 100 °C for 1 h. After cooling to room temp the solvents were removed under reduced pressure and the residue was purified by flash chromatography on silica gel (*n*-hexane/ethyl acetate) to give the analytically pure product **6**.

**Table 7.** Experimental details of the consecutive pseudo four-component synthesis of cyanines **6**.

Entry	Alkyne <b>7</b>	Amine <b>9c</b>	Yield <sup>a</sup>
1	140 $\mu\text{L}$ (0.98 mmol) of <b>7a</b>	85 $\mu\text{L}$ (1.00 mmol) of <b>9c</b>	209 mg (99%) of <b>6b</b>
2	110 $\mu\text{L}$ (1.00 mmol) of <b>7d</b>	85 $\mu\text{L}$ (1.00 mmol) of <b>9c</b>	214 mg (86%) of <b>6c</b>

<sup>a</sup> The yield refers to the employed amount of amine, i.e., two equivs of amine **9c** reacted with one equiv of compound **2**. The unreacted alkyne intermediate was not isolated.

#### 4.10. (E)-1-[5,5-Dimethyl-3-[2-(pyrrolidin-1-yl)vinyl]cyclohex-2-en-1-ylidene]pyrrolidin-1-ium (**6b**)

According to the GP, upon reaction of alkyne **7a** (140  $\mu\text{L}$ , 0.98 mmol) and pyrrolidine (**9c**) (85  $\mu\text{L}$ , 1.00 mmol) and after chromatography on silica gel (*n*-hexane/ethyl acetate/Net<sub>3</sub> 200:100:3) and drying under vacuum, compound **6b** (209 mg, 99%) was obtained as an orange solid, mp 180 °C,  $R_f$  (ethyl acetate): 0.05.

$^1\text{H}$  NMR (600 MHz, 298 K, acetone- $d_6$ ):  $\delta$  1.07 (s, 6 H), 1.97 (quint,  $J$  = 6.9 Hz, 3 H), 2.03 (s, 1 H), 2.09 (q,  $J$  = 7.1 Hz, 4 H), 2.55 (s, 2 H), 2.60 (s, 2 H), 3.46 (t,  $J$  = 7.2 Hz, 2 H), 3.64 (t,  $J$  = 6.8 Hz, 2 H), 3.69–3.85 (m, 4 H), 5.68 (d,  $J$  = 12.7 Hz, 1 H), 5.93 (s, 1 H), 8.08 (d,  $J$  = 12.6 Hz, 1 H).  $^1\text{H}$  NMR (600 MHz, 261 K, acetone- $d_6$ ):  $\delta$  1.04 (s, 6 H), 1.95 (t,  $J$  = 6.8 Hz, 2 H), 2.00–2.04 (m, 4 H), 2.06–2.10 (m, 2 H), 2.53 (s, 2 H), 2.59 (s, 2 H), 3.44 (t,  $J$  = 7.1 Hz, 2 H), 3.62 (t,  $J$  = 6.8 Hz, 2 H), 3.73 (t,  $J$  = 6.8 Hz, 2 H), 3.76 (t,  $J$  = 6.7 Hz, 2 H), 5.67 (d,  $J$  = 12.6 Hz, 1 H), 5.92 (s, 1 H), 8.09 (d,  $J$  = 12.6 Hz, 1 H).  $^{13}\text{C}$  NMR (151 MHz, 298 K, acetone- $d_6$ ):  $\delta$  25.2 ( $\text{CH}_2$ ), 25.5 ( $\text{CH}_2$ ), 25.6 ( $\text{CH}_2$ ), 28.2 ( $\text{CH}_3$ ), 32.6 ( $\text{C}_{\text{quat}}$ ), 38.9 ( $\text{CH}_2$ ), 42.7 ( $\text{CH}_2$ ), 48.3 ( $\text{CH}_2$ ), 50.5 ( $\text{CH}_2$ ), 54.1 ( $\text{CH}_2$ ), 104.1 ( $\text{CH}$ ), 104.9 ( $\text{CH}$ ), 122.2 ( $\text{C}_{\text{quat}}$ ,  $^1J_{\text{C-F}}$  = 322 Hz), 151.3 ( $\text{CH}$ ), 165.8 ( $\text{C}_{\text{quat}}$ ), 168.2 ( $\text{C}_{\text{quat}}$ ).  $^{13}\text{C}$  NMR (151 MHz, 261 K, acetone- $d_6$ ):  $\delta$  25.1 ( $\text{CH}_2$ ), 25.4 ( $\text{CH}_2$ ), 25.4 ( $\text{CH}_2$ ), 25.5 ( $\text{CH}_2$ ), 28.1 ( $\text{CH}_3$ ), 32.4 ( $\text{C}_{\text{quat}}$ ), 38.6 ( $\text{CH}_2$ ), 42.3 ( $\text{CH}_2$ ), 48.1 ( $\text{CH}_2$ ), 50.3 ( $\text{CH}_2$ ), 50.4 ( $\text{CH}_2$ ), 53.8 ( $\text{CH}_2$ ), 103.8 ( $\text{CH}$ ), 104.5 ( $\text{CH}$ ), 121.9 ( $\text{C}_{\text{quat}}$ ,  $^1J_{\text{C-F}}$  = 321 Hz), 151.1 ( $\text{CH}$ ), 165.4 ( $\text{C}_{\text{quat}}$ ), 167.8 ( $\text{C}_{\text{quat}}$ ). HR MS (ESI,  $m/z$  (%)) calcd for  $[\text{C}_{18}\text{H}_{29}\text{N}_2]^+$ : 273.2325 (100), 274.2359 (20), 275.2392 (2); Found: 273.2327 (100), 274.2359 (18), 275.2389

(2). IR:  $\tilde{\nu}$  [ $\text{cm}^{-1}$ ]: 2984 (w), 2957 (w), 2872 (w), 1624 (w), 1522 (m), 1477 (w), 1441 (m), 1412 (m), 1396 (w), 1375 (m), 1348 (m), 1337 (w), 1325 (w), 1262 (s), 1248 (s), 1233 (m), 1221 (s), 1152 (s), 1103 (m), 1026 (s), 1005 (w), 986 (w), 966 (w), 947 (w), 924 (w), 912 (w), 883 (m), 876 (m), 853 (m), 781 (w), 766 (w), 754 (w), 706 (w), 633 (s). UV/Vis ( $\text{CH}_2\text{Cl}_2$ ):  $\lambda_{\text{max}}$  [nm] ( $\epsilon$  [ $\text{L}\cdot\text{cm}^{-1}\cdot\text{mol}^{-1}$ ]): 443 (114000). Emission ( $\text{CH}_2\text{Cl}_2$ ):  $\lambda_{\text{max}}$  [nm]: 459. Stokes shift [ $\text{cm}^{-1}$ ]: 800. Anal calcd for  $\text{C}_{19}\text{H}_{29}\text{F}_3\text{N}_2\text{O}_3\text{S}$  (422.5): C 54.01, H 6.92, N 6.63, S 7.59; Found: C 54.04, H 7.21, N 6.54, S 7.48.

4.11.  $\epsilon$ -1-[5,5-Dimethyl-3-[2-phenyl-2-(pyrrolidin-1-yl)vinyl]cyclohex-2-en-1-yliden}pyrrolidin-1-ium (6c)

According to the GP, upon reaction of alkyne **7d** (110  $\mu\text{L}$ , 1.00 mmol) and pyrrolidine (**9c**) (85  $\mu\text{L}$ , 1.00 mmol) and after chromatography on silica gel (*n*-hexane/ethyl acetate/ $\text{NEt}_3$  200:100:3) and drying under vacuum, compound **6c** (214 mg, 86%) was obtained as an orange solid, mp 147  $^\circ\text{C}$ ,  $R_f$  (ethyl acetate/MeOH 3:1): 0.07.

$^1\text{H}$  NMR (600 MHz, 298 K,  $\text{DMSO}-d_6$ ):  $\delta$  0.83 (s, 6 H), 1.82–1.85 (m, 6 H), 1.94 (s, 2 H), 2.00–2.04 (m, 2 H), 2.33 (s, 2 H), 2.91 (s, 2 H), 3.19 (t,  $J = 7.9$  Hz, 2 H), 3.48–3.53 (m, 2 H), 3.60 (t,  $J = 7.7$  Hz, 2 H), 5.11 (s, 1 H), 5.52 (s, 1 H), 7.34–7.38 (m, 2 H), 7.45–7.78 (m, 3 H).  $^1\text{H}$  NMR (600 MHz, 298 K, acetone- $d_6$ ):  $\delta$  0.90 (s, 6 H), 1.89–1.96 (m, 6 H), 2.06–2.07 (m, 1 H), 2.08–2.09 (m, 1 H), 2.10–2.14 (m, 2 H), 2.41 (s, 2 H), 2.99 (s, 2 H), 3.28–3.36 (m, 2 H), 3.61–3.65 (m, 2 H), 3.65–3.73 (m, 2 H), 5.19 (s, 1 H), 5.57 (s, 1 H), 7.40–7.44 (m, 2 H), 7.58–7.66 (m, 3 H).  $^1\text{H}$  NMR (600 MHz, 261 K, acetone- $d_6$ ):  $\delta$  0.89 (s, 6 H), 1.91 (q,  $J = 6.9$  Hz, 6 H), 2.08–2.14 (m, 3 H), 2.40 (s, 2 H), 3.14 (s, 3 H), 3.24–3.38 (m, 2 H), 3.62 (s, 2 H), 3.67 (t,  $J = 7.0$  Hz, 2 H), 4.66 (s, 1 H), 5.15–6.24 (m, 1 H), 7.37–7.49 (m, 2 H), 7.56–7.70 (m, 3 H).  $^{13}\text{C}$  NMR (151 MHz, 298 K,  $\text{DMSO}-d_6$ ):  $\delta$  24.0 ( $\text{CH}_2$ ), 24.3 ( $\text{CH}_2$ ), 24.6 ( $\text{CH}_2$ ), 24.7 ( $\text{CH}_2$ ), 27.5 ( $\text{CH}_3$ ), 31.5 ( $\text{C}_{\text{quat}}$ ), 40.9 ( $\text{CH}_2$ ), 48.9 ( $\text{C}_{\text{quat}}$ ), 49.3 ( $\text{CH}_2$ ), 49.7 ( $\text{CH}_2$ ), 51.4 ( $\text{CH}_2$ ), 120.7 ( $\text{C}_{\text{quat}}$ , d,  $J_{\text{C-F}} = 322$  Hz), 127.2 (CH), 127.2 (CH), 129.7 (CH), 129.9 (CH), 129.9 (CH), 136.4 ( $\text{C}_{\text{quat}}$ ), 162.5 ( $\text{C}_{\text{quat}}$ ), 163.5 ( $\text{C}_{\text{quat}}$ ).  $^{13}\text{C}$  NMR (151 MHz, 298 K, acetone- $d_6$ ):  $\delta$  25.0 ( $\text{CH}_2$ ), 25.4 ( $\text{CH}_2$ ), 25.6 ( $\text{CH}_2$ ), 25.7 ( $\text{CH}_2$ ), 28.0 ( $\text{CH}_3$ ), 30.4 ( $\text{CH}_2$ ), 30.6 (CH), 32.5 ( $\text{C}_{\text{quat}}$ ), 42.3 ( $\text{CH}_2$ ), 50.0 ( $\text{CH}_2$ ), 50.4 ( $\text{CH}_2$ ), 50.7 ( $\text{CH}_2$ ), 52.4 ( $\text{CH}_2$ ), 122.4 ( $\text{C}_{\text{quat}}$ , q,  $J_{\text{C-F}} = 322$  Hz), 128.2 (CH), 130.7 (CH), 130.8 (CH), 137.8 ( $\text{C}_{\text{quat}}$ ), 164.2 ( $\text{C}_{\text{quat}}$ ), 165.0 ( $\text{C}_{\text{quat}}$ ), 167.0 ( $\text{C}_{\text{quat}}$ ).  $^{13}\text{C}$  NMR (151 MHz, 261 K, acetone- $d_6$ ):  $\delta$  24.9 ( $\text{CH}_2$ ), 25.2 ( $\text{CH}_2$ ), 25.3 ( $\text{CH}_2$ ), 25.5 ( $\text{CH}_2$ ), 25.6 ( $\text{CH}_2$ ), 27.8 ( $\text{CH}_3$ ), 30.3 ( $\text{CH}_2$ ), 30.6 (CH), 32.4 ( $\text{C}_{\text{quat}}$ ), 41.9 ( $\text{CH}_2$ ), 49.8 ( $\text{C}_{\text{quat}}$ ), 50.2 ( $\text{CH}_2$ ), 50.5 ( $\text{CH}_2$ ), 52.3 ( $\text{CH}_2$ ), 52.3 ( $\text{C}_{\text{quat}}$ ), 55.0 (CH), 101.9 (CH), 122.1 ( $\text{C}_{\text{quat}}$ , q,  $J_{\text{C-F}} = 322$  Hz), 127.9 (CH), 130.7 (CH), 137.6 ( $\text{C}_{\text{quat}}$ ), 164.6 ( $\text{C}_{\text{quat}}$ ). ESI MS calcd for  $[\text{C}_{24}\text{H}_{33}\text{N}_2]^+$ : 349.5; Found: 349.7; calcd for  $[\text{CF}_3\text{O}_3\text{S}]^-$ : 149.1; Found: 149.1. HR MS (ESI,  $m/z$  (%)) calcd for  $[\text{C}_{24}\text{H}_{33}\text{N}_2]^+$ : 349.2638 (100), 350.2672 (26); Found: 349.2640 (100), 350.2671 (18). IR:  $\tilde{\nu}$  [ $\text{cm}^{-1}$ ] = 2955 (w), 2922 (w), 2872 (w), 1526 (w), 1504 (m), 1495 (m), 1472 (m), 1439 (m), 1410 (m), 1383 (m), 1346 (w), 1319 (m), 1292 (w), 1261 (s), 1238 (m), 1219 (s), 1180 (m), 1138 (s), 1105 (m), 1028 (s), 999 (w), 953 (w), 922 (w), 914 (w), 881 (m), 864 (m), 845 (m), 820 (m), 793 (w), 772 (m), 752 (w), 706 (w), 692 (m), 635 (s), 611 (m). UV/Vis ( $\text{CH}_2\text{Cl}_2$ ):  $\lambda_{\text{max}}$  [nm] ( $\epsilon$  [ $\text{L}\cdot\text{cm}^{-1}\cdot\text{mol}^{-1}$ ]): 459 (130000). Emission ( $\text{CH}_2\text{Cl}_2$ ):  $\lambda_{\text{max}}$  [nm]: 513. Stokes shift [ $\text{cm}^{-1}$ ]: 2300. Anal calcd for  $\text{C}_{25}\text{H}_{33}\text{F}_3\text{N}_2\text{O}_3\text{S}$  (498.6): C 60.22, H 6.67, N 5.62, S 6.43; Found: C 60.27, H 6.75, N 5.56, S 6.16.

**Supplementary Materials:** The following are available online at <https://www.mdpi.com/article/10.3390/photochem2030044/s1>. Figure S1: Three kinds of helix chains constitute the channel column of NUM-14. Figure S2: Comparison of simulated, experimental, and activated PXRD patterns of NUM-14. Figure S3: TGA curve for NUM-14 under Ar atmosphere. Figure S4: The PXRD patterns for NUM-14 after immersed in common solvents a week. Figure S5: The details of Virial equation (solid lines) fitting to the experimental  $\text{C}_2\text{H}_2$  adsorption data (symbols) for NUM-14a. Figure S6: The details of Virial equation (solid lines) fitting to the experimental  $\text{CO}_2$  adsorption data (symbols) for NUM-14a. Figure S7: The details of Virial equation (solid lines) fitting to the experimental  $\text{C}_2\text{H}_4$  adsorption data (symbols) for NUM-14a. Figure S8: The details of dual-site Langmuir-Freundlich isotherm (solid lines) fitting to the experimental  $\text{C}_2\text{H}_2$  adsorption data (symbols) for NUM-14a at 273 K. Figure S9: The details of dual-site Langmuir-Freundlich isotherm (solid lines) fitting to the

experimental C<sub>2</sub>H<sub>2</sub> adsorption data (symbols) for NUM-14a at 298 K. Figure S10: The details of single-site Langmuir-Freundlich isotherm (solid lines) fitting to the experimental CO<sub>2</sub> adsorption data (symbols) for NUM-14a at 273 K. Figure S11: The details of single-site Langmuir-Freundlich isotherm (solid lines) fitting to the experimental CO<sub>2</sub> adsorption data (symbols) for NUM-14a at 298 K. Figure S12: The details of dual-site Langmuir-Freundlich isotherm (solid lines) fitting to the experimental C<sub>2</sub>H<sub>4</sub> adsorption data (symbols) for NUM-14a at 273 K. Figure S13: The details of dual-site Langmuir-Freundlich isotherm (solid lines) fitting to the experimental C<sub>2</sub>H<sub>4</sub> adsorption data (symbols) for NUM-14a at 298 K. Table S1: Crystal data and structure refinement parameters for NUM-14 [46–49].

**Author Contributions:** The work consists of parts of the Ph.D. thesis of J.P., which is supervised by T.J.J.M. and the B.Sc. thesis of T.G., which was supervised by J.P. The conceptualization was outlined and accompanied by T.J.J.M. Synthetic studies were performed by J.P. and T.G. All analytical assignments and photophysical investigations were performed by J.P. The crystal structure analysis was performed and solved by G.J.R. The DFT and TDDFT computations and interpretations were performed by B.M. Writing—original draft preparation, J.P.; writing—review and editing, T.J.J.M.; project administration and funding acquisition was done by T.J.J.M. All authors have read and agreed to the published version of the manuscript.

**Funding:** This research was funded by Deutsche Forschungsgemeinschaft (Mu 1088/9-1) and the Fonds der Chemischen Industrie.

**Institutional Review Board Statement:** Not applicable.

**Informed Consent Statement:** Not applicable.

**Data Availability Statement:** Data (spectra and computational input files) are collected in the Supplementary Materials of this article.

**Acknowledgments:** We cordially thank the Deutsche Forschungsgemeinschaft (Mu 1088/9-1) and the Fonds der Chemischen Industrie for financial support. Computational support and infrastructure were provided by the “Centre for Information and Media Technology” (ZIM) at the University of Düsseldorf (Germany). We thank CeMSA@HHU (Center for Molecular and Structural Analytics @ Heinrich Heine University) for recording the mass-spectrometric and the NMR-spectroscopic data.

**Conflicts of Interest:** The authors declare no conflict of interest.

## References

1. Shindy, H. Fundamentals in the chemistry of cyanine dyes: A review. *Dye. Pigment.* **2017**, *145*, 505–513. [\[CrossRef\]](#)
2. Panigrahi, M.; Dash, S.; Patel, S.; Mishra, B.K. Syntheses of cyanines: A review. *Tetrahedron* **2012**, *68*, 781–805. [\[CrossRef\]](#)
3. Kulinich, A.V.; Ishchenko, A.A. Merocyanine dyes: Synthesis, structure, properties and applications. *Russ. Chem. Rev.* **2009**, *78*, 141–164. [\[CrossRef\]](#)
4. Shirinian, V.Z.; Shimkin, A.A. Merocyanines: Synthesis and Application. *Top. Heterocycl. Chem.* **2008**, *14*, 75–105. [\[CrossRef\]](#)
5. Mishra, A.; Behera, R.K.; Behera, P.K.; Mishra, B.K.; Behera, G.B. Cyanines during the 1990s: A Review. *Chem. Rev.* **2000**, *100*, 1973–2012. [\[CrossRef\]](#) [\[PubMed\]](#)
6. Hamer, F.M. *The Cyanine Dyes and Related Compounds*; Interscience: New York, NY, USA; London, UK, 1964.
7. Kim, T.-D.; Lee, K.-S. D- $\pi$ -A Conjugated Molecules for Optoelectronic Applications. *Macromol. Rapid Commun.* **2015**, *36*, 943–958. [\[CrossRef\]](#)
8. Castet, F.; Rodriguez, V.; Pozzo, J.-L.; Ducasse, L.; Plaquet, A.; Champagne, B. Design and Characterization of Molecular Nonlinear Optical Switches. *Acc. Chem. Res.* **2013**, *46*, 2656–2665. [\[CrossRef\]](#)
9. Marder, S.R. Organic nonlinear optical materials: Where we have been and where we are going. *Chem. Commun.* **2005**, *37*, 131–134. [\[CrossRef\]](#)
10. Würthner, F.; Wortmann, R.; Meerholz, K. ChemInform Abstract: Chromophore Design for Photorefractive Organic Materials. *ChemInform* **2010**, *33*, 17–31. [\[CrossRef\]](#)
11. Gsänger, M.; Bialas, D.; Huang, L.; Stolte, M.; Würthner, F. Organic Semiconductors based on Dyes and Color Pigments. *Adv. Mater.* **2016**, *28*, 3615–3645. [\[CrossRef\]](#)
12. Arjona-Esteban, A.; Lenze, M.R.; Meerholz, K.; Würthner, F. Donor-Acceptor Dyes for Organic Photovoltaics. In *Elementary Processes in Organic Photovoltaics*; Advances in Polymer Science; Leo, K., Ed.; Springer: Berlin/Heidelberg, Germany, 2017; Volume 2726, pp. 193–214.
13. Würthner, F. Dipole-Dipole Interaction Driven Self-Assembly of Merocyanine Dyes: From Dimers to Nanoscale Objects and Supramolecular Materials. *Accounts Chem. Res.* **2016**, *49*, 868–876. [\[CrossRef\]](#) [\[PubMed\]](#)

14. Heyne, B. Self-assembly of organic dyes in supramolecular aggregates. *Photochem. Photobiol. Sci.* **2016**, *15*, 1103–1114. [[CrossRef](#)] [[PubMed](#)]
15. Kovtun, Y. Metallochromic merocyanines of 8-hydroxyquinoline series. II. Dyes with end nuclei of low basicity. *Dye. Pigment.* **2004**, *60*, 215–221. [[CrossRef](#)]
16. Kovtun, Y.; Prostota, Y.; Tolmachev, A. Metallochromic merocyanines of 8-hydroxyquinoline series. *Dye. Pigment.* **2003**, *58*, 83–91. [[CrossRef](#)]
17. Yagi, S.; Maeda, K.; Nakazumi, H. Photochromic properties of cationic merocyanine dyes. Thermal stability of the spiropyran form produced by irradiation with visible light. *J. Mater. Chem.* **1999**, *9*, 2991–2997. [[CrossRef](#)]
18. Levi, L.; Müller, T.J.J. Multicomponent syntheses of functional chromophores. *Chem. Soc. Rev.* **2016**, *45*, 2825–2846. [[CrossRef](#)]
19. Müller, T.J.J.; Bunz, U.H.F. (Eds.) *Functional Organic Materials*; Wiley-VHC: Weinheim, Germany, 2007.
20. Levi, L.; Müller, T.J.J. Multicomponent Syntheses of Fluorophores Initiated by Metal Catalysis. *Eur. J. Org. Chem.* **2016**, *2016*, 2902–2918. [[CrossRef](#)]
21. Zhu, J.; Wang, Q.; Wang, M.-X. (Eds.) *Multi-Component Reactions in Organic Synthesis*; Wiley-VHC: Weinheim, Germany, 2015.
22. Müller, T.J.J. Relative Reactivities of Functional Groups as the Key to Multicomponent Reactions. In *Science of Synthesis Series: Multicomponent Reactions 1—General Discussion and Reactions Involving a Carbonyl Compound as Electrophilic Component*; Müller, T.J.J., Ed.; Georg Thieme: Stuttgart, Germany, 2014; pp. 5–27. [[CrossRef](#)]
23. D'Souza, D.M.; Müller, T.J.J. Multi-component syntheses of heterocycles by transition-metal catalysis. *Chem. Soc. Rev.* **2007**, *36*, 1095–1108. [[CrossRef](#)] [[PubMed](#)]
24. Dömling, A.; Ugi, I. Multicomponent Reactions with Isocyanides. *Angew. Chem. Int. Ed.* **2000**, *39*, 3169–3210. [[CrossRef](#)]
25. D'Souza, D.M.; Kiel, A.; Herten, D.-P.; Rominger, F.; Müller, T.J.J. Synthesis, Structure and Emission Properties of Spirocyclic Benzofuranones and Dihydroindolones: A Domino Insertion-Coupling-Isomerization-Diels-Alder Approach to Rigid Fluorophores. *Chem. A Eur. J.* **2007**, *14*, 529–547. [[CrossRef](#)]
26. D'Souza, D.M.; Rominger, F.; Müller, T.J.J. A Domino Sequence Consisting of Insertion, Coupling, Isomerization, and Diels-Alder Steps Yields Highly Fluorescent Spirocycles. *Angew. Chem. Int. Ed.* **2004**, *44*, 153–158. [[CrossRef](#)] [[PubMed](#)]
27. Gers-Panther, C.F.; Müller, T.J.J. Multicomponent Syntheses of Heterocycles Initiated by Catalytic Generation of Ynones and Ynediones. In *Advances in Heterocyclic Chemistry: Heterocyclic Chemistry in the 21st Century: A Tribute to Alan Katritzky*; Scriven, E.F.V., Ramsden, C.A., Eds.; Elsevier: Amsterdam, The Netherlands, 2016; Volume 120, pp. 67–98.
28. Müller, T.J.J. Multi-component synthesis of fluorophores via catalytic generation of alkynoyl intermediates. *Drug Discov. Today Technol.* **2018**, *29*, 19–26. [[CrossRef](#)] [[PubMed](#)]
29. Muschelknautz, C.; Frank, W.; Müller, T.J.J. Rapid Access to Unusual Solid-State Luminescent Merocyanines by a Novel One-Pot Three-Component Synthesis. *Org. Lett.* **2011**, *13*, 2556–2559. [[CrossRef](#)]
30. Papadopoulos, J.; Merckens, K.; Müller, T.J.J. Three-Component Synthesis and Photophysical Properties of Novel Coumarin-Based Merocyanines. *Chem.—A Eur. J.* **2017**, *24*, 974–983. [[CrossRef](#)]
31. Pasch, P.; Papadopoulos, J.; Goralczyk, A.; Hofer, M.L.; Tabatabai, M.; Müller, T.J.J.; Hartmann, L. Highly Fluorescent Merocyanine and Cyanine PMMA Copolymers. *Macromol. Rapid Commun.* **2018**, *39*, e1800277. [[CrossRef](#)]
32. Papadopoulos, J.; Müller, T.J.J. Rapid synthesis of 4-alkynyl coumarins and tunable electronic properties of emission solvatochromic fluorophores. *Dye. Pigment.* **2019**, *166*, 357–366. [[CrossRef](#)]
33. Krefß, K.C.; Fischer, T.; Stumpe, J.; Frey, W.; Raith, M.; Beiraghi, O.; Eichhorn, S.H.; Tussetschlager, S.; Laschat, S. Influence of Chromophore Length and Acceptor Groups on the Optical Properties of Rigidified Merocyanine Dyes. *ChemPlusChem* **2013**, *79*, 223–232. [[CrossRef](#)] [[PubMed](#)]
34. Hoang, T.T.; Birepinte, M.; Kramer, N.J.; Dudley, G.B. Six-Step Synthesis of Alcyopterosin A, a Bioactive Illudalane Sesquiterpene with a gem-Dimethylcyclopentane Ring. *Org. Lett.* **2016**, *18*, 3470–3473. [[CrossRef](#)]
35. Morrison, A.E.; Hrudka, J.J.; Dudley, G.B. Thermal Cycloisomerization of Putative Allenylpyridines for the Synthesis of Isoquinoline Derivatives. *Org. Lett.* **2016**, *18*, 4104–4107. [[CrossRef](#)]
36. Deposition Number CCDC 2183900 Contains the Supplementary Crystallographic Data for This Paper. These Data are Provided Free of Charge by the Joint Cambridge Crystallographic Data Centre and Fachinformationszentrum Karlsruhe. Available online: <http://www.ccdc.cam.ac.uk/structures> (accessed on 30 June 2022).
37. Marder, S.R.; Gorman, C.B.; Tiemann, B.G.; Perry, J.W.; Bourhill, G.; Mansour, K. Relation Between Bond-Length Alternation and Second Electronic Hyperpolarizability of Conjugated Organic Molecules. *Science* **1993**, *261*, 186–189. [[CrossRef](#)]
38. Muroph, H. Polymethine dyes. *Phys. Sci. Rev.* **2019**, *5*, 5648–5652. [[CrossRef](#)]
39. Becke, A.D. Density-functional thermochemistry. III. The role of exact exchange. *J. Chem. Phys.* **1993**, *98*, 5648–5652. [[CrossRef](#)]
40. Ernzerhof, M.; Perdew, J.P. Generalized gradient approximation to the angle- and system-averaged exchange hole. *J. Chem. Phys.* **1998**, *109*, 3313–3320. [[CrossRef](#)]
41. Yanai, T.; Tew, D.; Handy, N.C. A new hybrid exchange-correlation functional using the Coulomb-attenuating method (CAM-B3LYP). *Chem. Phys. Lett.* **2004**, *393*, 51–57. [[CrossRef](#)]
42. Krishnan, R.; Binkley, J.S.; Seeger, R.; Pople, J.A. Self-consistent molecular orbital methods. XX. A basis set for correlated wave functions. *J. Chem. Phys.* **1980**, *72*, 650–654. [[CrossRef](#)]



- 
43. Caricato, M.; Mennucci, B.; Tomasi, J.; Ingrosso, F.; Cammi, R.; Corni, S.; Scalmani, G. Formation and relaxation of excited states in solution: A new time dependent polarizable continuum model based on time dependent density functional theory. *J. Chem. Phys.* **2006**, *124*, 124520. [[CrossRef](#)]
  44. Frisch, M.J.; Trucks, G.W.; Schlegel, H.B.; Scuseria, G.E.; Robb, M.A.; Cheeseman, J.R.; Scalmani, G.; Barone, V.; Petersson, G.A.; Nakatsuji, H.; et al. *Gaussian 16, Revision C.01*; Gaussian, Inc.: Wallingford, CT, USA, 2016.
  45. Jacquemin, D.; Zhao, Y.; Valero, R.; Adamo, C.; Ciofini, I.; Truhlar, D.G. Verdict: Time-Dependent Density Functional Theory “Not Guilty” of Large Errors for Cyanines. *J. Chem. Theory Comput.* **2012**, *8*, 1255–1259. [[CrossRef](#)]
  46. Bruker. *Saint, Apex2, Sadabs*; Bruker AXS Inc.: Madison, WI, USA, 2011.
  47. Sheldrick, G.M. A short history of SHELX. *Acta Crystallogr. Sect. A Found. Crystallogr.* **2008**, *71*, 112–122.
  48. Sheldrick, G.M. Crystal structure refinement with SHELXL. *Acta Crystallogr. Sect. C Struct. Chem.* **2015**, *71*, 3–8.
  49. Brandenburg, K. *DIAMOND 4.6.4*, Bonn, Germany, 2018.